Investigation of the dB/dH Effect using Trapped Flux in Type II Superconductors

by

Sean X. Wang

Thesis submitted to the School of Graduate Studies and Research

of the University of Ottawa in partial fulfillment

of the requirements for the degree

of Master of Science in Physics

Department of Physics

University of Ottawa

Ottawa, Canada

ISBN 0-315-83847-7

Canada

UNIVERSITÉ D'OTTAWA
UNIVERSITY OF OTTAWA

ACKNOWLEDGEMENTS

I would like to express my sincere appreciation and gratitude to Dr.Marcel A.R. LeBlanc for his constant, patient and excellent guidance which made my dreams and hopes of research in materials science and physics come true at last in Canada. His dedication to research and pursuit of knowledge exceeds all my expectations.

Finally, I wish to thank my wife for her self-sacrifice throughout this project.

ABSTRACT

Many workers visualize that, when magnetic flux first penetrates into type II superconductors, the flux line lattice exhibits a discontinuity of magnitude comparable to the lower critical field H_{c1} over a dimension of the order of the penetration depth λ along the front of the invading flux line lattice. This discontinuity is referred to as the dB/dH effect in the literature. Such a discontinuity is also thought to exist in the magnetic flux configuration (B profile) at the periphery of the specimen when the applied magnetic field H_a, which caused the flux lines to enter the specimen, is then removed.

We have compared $< B >_{rem}$, the amount of magnetic flux trapped in a sample after it has been subjected to an excursion (half cycle) of H_a with $< B >_{in}$, the amount of flux permeating the specimen at the peak of a half cycle of H_a. Such measurements were performed on six conventional type II supercondutors in the form of long solid cylinders and ribbons.

These observations are compared with critical state model predictions which incorporate discontinuities in the B profile of various magnitude ranging from zero to B_{c1} and beyond. We show that the presence of any such discontinuities will be dramatically evident in graphs of $< B >_{rem}/ < B >_{in}$ versus $< B >_{in}$. Plots of the data in this format indicate quite clearly that discontinuities are not present.

Contents

List of Figures

List of Tables

Chapter 1

Introduction

1-1 General Statement

Type II superconductivity has become an integral part of our knowledge of nature for three decades already. Nevertheless some major features in the behaviour of these materials in the range of weak applied magnetic fields $H_a \lesssim H_{c1}$ still remain qualitatively unexplained.(H_{c1} is the critical field for first entry of magnetic flux in the bulk of a specimen). For instance, according to the accepted theoretical picture, the magnetic flux density in the body of these materials (hence excepting the small penetration depth regime) should remain unchanged as H_a is varied between $+H_{c1}$ and $-H_{c1}$. However this idealized response is seldom if ever encountered in the real samples when the previous field-temperature (H_a-T) history has introduced magnetic flux in the superconducting

specimen. Indeed, in these circumstances, the 'work horse' of large scale applications of superconductivity, NbTi, exhibits a rapid decrease of the magnetic flux threading the specimens as H_a approaches zero.

Also there is no universally accepted picture of the configuration of the magnetic flux density in type II superconductors in the range of weak applied magnetic fields. In particular, several researchers visualize that the magnetic flux density decreases abruptly from $B(x) \approx B_{c1}$ to zero over a distance of the order of the penetration depth λ far inside the body of the specimen when an increase in H_a beyond H_{c1} has caused magnetic flux to penetrate into the volume of the sample.[12, 13, 15, 16, 20, 25, 28, 32] This 'discontinuity' in the magnetic flux density profile is known as the dB/dH effect.[5, 6, 7, 9, 29] Many workers, however, do not consider the existence of such a sudden change or 'discontinuity' in the configuration of magnetic flux density in the analysis of their data on critical currents, hysteresis losses and magnetic response of type II superconductors. In this thesis we address this as yet unresolved matter.

1-2 Background

The capacity of type II superconductors to support lossless currents in the presence of strong magnetic fields is not only a fundamental property of these materials but, undoubtedly, the feature which makes these materials interesting and important for various

practical applications. It is therefore not surprising that a considerable effort has been dedicated in numerous laboratories to the determination of the maximum lossless or critical current I_c which a specimen can sustain as a function of applied magnetic field H_a and temperature T. Since I_c versus H_a at a fixed T is very sensitive to the mode of preparation and subsequent treatment of a material of specified chemical composition , the situation is somewhat complicated. For engineering purposes,however, it may be sufficient to simply catalogue curves of I_c vs H_a for various chosen T for different materials and for the several useful fabrication procedures. It is essential for progress and understanding that the basic factors which affect I_c be well identified and elucidated.

Since the critical current I_c depends on the size and geometry of a specimen, it is more convenient in characterizing a material to focus on the critical current density j_c. Because I_c generally varies with H_a, it is expected that j_c will depend on the magnetic flux density B. Further, j_c will generally not be uniform in a specimen even though the material is homogeneous, isotropic and uniform in its properties. The reason for this is that by Maxwell's equation, $\nabla \times \vec{B} = \mu_0 \vec{j}$, the current flowing in the sample will cause B to vary spatially in magnitude as well as in orientation.

Two different approaches have been exploited to determine I_c hence j_c . They are denoted as the 'four probe' technique and the 'magnetic' method. We now outline both of these schemes.

The 'four probe' technique is conceptually simple although not always straightforward in implementation. Current leads are attached to the ends of the specimen and connected to a current source. Voltage leads are secured to the specimen at two positions located between the current connections and some distance from the latter. It is important that the cross section S of the specimen between the voltage leads be uniform and accuratedly known. The onset of a voltage detected by a sensitive voltmeter between these leads as I is impressed determines I_c. Thus the spatial average, $< j_c >= I_c/S$ is readily obtained vs H_a and T. Since the sensitivity of voltmeters is limited, the accuracy of these measurements diminishes as the length of the specimen is diminished and the cross section is enlarged. The main problem with this technique arises from the fact that a contact resistance R_c inevitably exists between the current leads and the superconducting specimen. Joule (i.e.I^2R_c) heating at the two interfaces causes the temperature of the superconducting material in their vicinity to rise, thereby severely disturbing the superconducting state and its lossless current carrying capacity. Much effort and skill have been devoted to minimizing R_c and to diminishing its effects. The magnitudes of the critical currents and current densities coming into play in the most technologically promising materials are so large however, particularly in the range of low and weak fields, that the best contacts continue to present a major obstacle in these circumstances.

Partly to circumvent the contact 'bottleneck' and also to obtain complementary data,

a variety of 'magnetic' schemes have been devised and explored. The essential features of these various methods are also relatively straightforward.

By Faraday's law of induction, a change $\Delta\Phi$, of the magnetic flux threading a specimen generates an emf ε, hence an electric field E related to ε by the definition $\varepsilon = \oint \vec{E} \cdot d\vec{l}$. The electric field E(t) accelerates the superelectrons (Cooper pairs of density n^* and charge e^*) giving rise to a current density,

$$j = n^* e^* v \tag{1.1}$$

which grows until a critical value j_c is attained where dissipation of kinetic energy begins to take place by various processes. Hence an effective resistivity appears in the superconducting state until j decays infinitesimally below the critical value. After the increment (or decrement) $\Delta\ H_a$ of the applied field has taken place, a steady state ensues where a pattern of circulating induced current density is established at the threshold (critical) value over part or all of the volume of the specimen.

We recall that an element of current,

$$\Delta I = \vec{j} \cdot \Delta\vec{S} \tag{1.2}$$

flowing around the periphery of an area A constitutes an elementary magnetic moment or magnetic dipole,

$$\Delta\mu = (\Delta I)A = (\vec{j} \cdot \Delta\vec{S})A \tag{1.3}$$

Thus, the persistent circulating currents induced by the change of H_a cause the specimen to develop a magnetic moment

$$\mu = \int d\mu = \int (\vec{j} \cdot d\vec{S}) A \tag{1.4}$$

which can be measured by a variety of schemes and instruments (eg. vibrating sample magnetometer, SQUID magnetometer). The magnetic moment μ or the magnetization,

$$< M >= \frac{\mu}{V} \tag{1.5}$$

where V is the volume of the specimen, yield information on j_c vs H_a.

In our work, we have exploited the magnetic method because it is considerably more convenient for the low field range applicable in our thesis. Further, this approach besides providing data on j_c vs B, also yields information on the configuration of the magnetic flux density which cannot be obtained from 'four probe' measurements.

Chapter 2

Framework of Our Investigation

2-1 Main Purpose of the Investigation

There is at present no universally accepted picture of the configuration of magnetic flux in nonideal (irreversible) type II superconductors in the low field range. The chief objective of the work reported in this thesis is to shed some light on this confused situation and try to identify the correct answer. First we outline the well established elements of the picture and then indicate the controversial features.

When a magnetic field H_a is impressed upon a virgin (zero field cooled) type II superconducting specimen of negligible demagnetization factor, screening persistent currents are induced to flow around the periphery of the sample in a surface region denoted as the penetration depth λ. Typically, $\lambda \approx 10^3 \mathring{A}$ when $T/T_c \leq 0.8$. If the specimen possesses no

surface barrier, entry of flux lines into the bulk of the sample will commence when H_a exceeds H_{c1}. In the event that the sample has a surface barrier, entry of flux lines will begin to take place when H_a exceeds $(H_{c1}+\Delta H_{en})$, where ΔH_{en} denotes the height of the barrier against flux entry [8, 18]. By Maxwell's equation, $\nabla \times \vec{H} = \mu_0 \vec{j}$, or equivalently, Ampere's law, $\oint \vec{H} \cdot d\vec{l} = I$, a surface current per unit length, I_{c1}=H_{c1} is associated with H_{c1} and a surface current per unit length, $I_b = \Delta H_{en}$ is associated with ΔH_{en}. When the dimensions of the specimen are large compared with λ and with the thickness of the surface barrier λ_b, the magnetic flux threading λ and λ_b can be neglected. In this thesis,we consider such large samples, hence, only the magnetic flux threading the bulk of the specimen will be taken into account.

We let B(x) denote the flux line density in the bulk (body or volume) of the specimen. B(x) is a quasi-microscopic average over the cross section of a few flux lines. It is generally accepted that the B profile (i.e. the configuration of the flux line lattice) which has penetrated into the specimen exists in a critical state when the driving Lorentz force F_L acting on the flux lines is in equilibrium with the opposing pinning force F_p due to physical imperfections and chemical impurities etc. This concept is often called the Bean model in the recent literature although it was developed by Bean, London, Kim and Anderson [2, 3, 4, 14, 19]. We will use the expression, critical state model (abbreviated to CSM) for historical accuracy and also because we will use the name Bean in another context in this

thesis.

Combining the critical state model (CSM) with Maxwell's equation leads to the statement,

$$\nabla \times \vec{B} = \mu_0 \vec{j_c} \tag{2.1}$$

where j_c depends on B,T and parameters characterizing the specimen and material. The foregoing is generally accepted and established.

The controversial point which we want to address in this thesis concerns the 'structure' at the front of the advancing flux line lattice inside the specimen. To fix ideas and for simplicity, we consider an infinite slab of thickness 2X with surfaces situated at $x = \pm X$ and with $\vec{H}_a$, hence $\vec{B}(x)$, directed along the z axis. For brevity, coordinate subscripts will be omitted. The current density j_c, hence the current, flows along the + or − y axis. B and j_c will generally vary with x but not with y and z since we are stipulating idealized infinite slab (planar) geometry.

Many workers visualize that the flux line density, B(x), hence the B profile diminishes monotonically from its value $B_s(\pm X)$ just inside the surfaces of the specimen to zero at the front of the B profile, until $B_s = B_*$, where B_* denotes the full penetration field. We refer the reader to Fig.2.1 for aid in visualizing the prevailing picture. Since j_c can be very large when B is small, and equation (2.1) for planar geometry reads,

$$\frac{dB}{dx} = \pm \mu_0 j_c(x) \tag{2.2}$$

it is evident that the slope of the B profile will be quite steep at the front of the B profile.

Several workers [12, 13, 15, 16, 20, 25, 28, 32], however, have proposed that a 'discontinuity' on a quasi-microsocopic scale should appear at the front of the advancing B profile. This feature is sometimes referred to as the 'dB/dH' effect [5, 6, 7, 9, 29]. In other words, across this quasi-microscopic region, μ_0H(x) should vary from zero at one edge to $\mu_0 H_{c1} = B_{c1}$ over a distance of the order of the penetration depth λ. We note that if $B_{c1} \approx$ 10 mT, this corresponds to a current density $< j_c > \approx 10^{11} A/m^2$ at the front of the B profile (since $B_{c1} \approx$ 100 mT for Nb, here $< j_c > \approx 10^{12} A/m^2$). Since pinning may cause some disorder and irregularity in the flux line lattice and for various other reasons, some proponents of a 'discontinuity' at the front of the B profile, have stipulated or proposed or conjectured that the 'discontinuity' could range anywhere from a fraction f of B_{c1} to the full value of B_{c1} [16], but be constant for a given specimen at a fixed T. The corresponding configuration of the B profile is displayed in Fig.2.1(d). The figures are grouped at the end of the chapter for convenience of consultation as a sequence since they complement each other.

As the externally applied magnetic field is increased , the flux fronts advance from the left and right surfaces and eventually meet at the midplane as depicted in Figs.2.1(b) and (e). We let B_* denote the magnetic flux density just inside the surface(s) when this collision or junction occurs. In the model where no discontinuity is envisaged, equation

(2.2) leads to,

$$B_* = B'_* = \mu_0 \int_0^X j_c(x)dx \tag{2.3}$$

whereas if a discontinuity is stipulated,

$$B_* = B''_* = fB_{c1} + \mu_0 \int_0^X j_c(x)dx \tag{2.4}$$

where the prime and double prime are used to distinguish between the two situations.

The B profiles evolve as shown in Figs.2.1(c) and (f) as H_a is increased beyond the full penetration value H_a^*. The B profiles in the two cases are qualitatively identical when $H_a > H_a^*$. In the no discontinuity model,however, there is a range of H_a from 0 to H_a^* where B at the midplane (B(x =0)), grows gradually from 0 to fB_{c1} whereas in the discontinuity model, B(x =0) 'jumps' abruptly from 0 to fB_{c1} when the fronts meet.

Our purpose in this investigation is to determine which of these two models corresponds to reality.

Evidently, if a microprobe measuring flux line density could be inserted in the specimen, the matter would be unambiguously resolved. Unfortunately, Hall effect or magnetoresistance probes, minute enough to accomplish this, do not exist. Further the probe has to be inserted in a cavity drilled in the specimen. The cavity is a normal region which seriously perturbs the configuration of the magnetic flux in its vicinity. Hence, the probe observes a severely disturbed profile. Nevertheless,measurements of the 'coarse' distribution of the magnetic flux density have been performed[29]. Alternative schemes

have to be devised to elucidate this question. We follow the lead of many workers [10, 11, 13, 17, 21, 22, 23, 24, 26, 27, 28, 33] and exploit measurements of the residual magnetic flux trapped in the specimen, also called the remanent flux, to provide the answer. We introduce a novel feature in this approach which is more discriminating or sensitive to the presence or absence of the discontinuity, than the standard method heretofore utilised.

2-2 Remanent Magnetization

Two straightforward procedures have usually been followed to establish a residual (remanent) magnetic moment in type II superconductors. We refer the reader to Fig.2.2 which displays these two procedures in the H-T phase. These are called the zero field cooled (Z.F.C.) and field cooled (F.C.) procedures.

2-2-1 Zero Field Cooled (ZFC) Procedure

In the zero field cooled (ZFC) method, the specimen is cooled from above T_c to some selected temperature $T_f < T_c$ in no applied magnetic field. Generally the earth's magnetic field is considered negligible, hence zero, in these experiments and is not cancelled. Now with the sample maintained at T_f, the specimen is subjected to a slow sweep of an externally applied magnetic field H_a up to some chosen value, which we denote H_{cycle}. H_{cycle}

is maintained constant for some time, generally several seconds and then H_a is gradually removed.

Evidently, the magnetic moment μ, hence the magnetization $M = \mu/V$, generated as H_a is impressed and subsequently removed can be monitored throughout this 'half' cycle of H_a. Thus the actual measurements need not be confined to the determination of the ensuing residual (remanent) value. We let μ_{rem} and $< M >_{rem}$ denote, the remanent magnetic moment and corresponding magnetization. In our work, μ, hence M, is indeed continuously monitored as H_a is impressed and removed. Typical locus of $< B >$, the spatial average of the magnetic flux density and of the magnetization $< M >$ are displayed in Fig.2.3 as H_a is applied up to $H_{cycle} \equiv H''_{cycle} > H_{c1} + \Delta H_{en}$ and then reduced to zero.

Clearly, if $H_{cycle} = H'_{cycle} < H_{c1} + \Delta H_{en}$, no magnetic flux enters the specimen (except in the penetration depths λ and λ_b which are negligible), hence then, $< B >_{rem} = 0$ and $< M >_{rem} = 0$. We note for completeness that any magnetic flux occupying the penetration depth λ when $H_a = H_{cycle}$, will be released (thermodynamic reversibility) when H_a is reduced to zero. The fate of the magnetic flux which occupied the depth of the surface barrier λ_b when H_{cycle} was present is another matter. Whether any of this flux remains in the surface barrier space after H_a has been removed is a question yet to be answered.

Fig.2.3 also illustrates the fact that $< B >_{rem}$, hence $< M >_{rem}$ increase monotonically

as,

$$H_{cycle} = H''_{cycle} > \qquad H_{c1} + \Delta H_{en} \tag{2.5}$$

is made larger. Further, Fig.2.3 also depicts the important feature that $< B >_{rem}$ attains a maximum value $< B >_{remmax}$, hence $< M >_{rem}$ grows to a maximum or saturation value $< M >_{remmax}$ when H''_{cycle} exceeds a threshold value, denoted as H^{**}_{cycle}. Consequently, it is expected and observed that $< M >_{rem}$ vs H_{cycle} will traverse or display three regimes of behaviour, namely,

$$< M >_{rem} = 0, \qquad H_{cycle} < H_{c1} + \Delta H_{en} \tag{2.6}$$

$$0 < \ < M >_{rem} \ < \ < M >_{remmax}, \qquad H_{c1} + \Delta H_{en} < H_{cycle} < H^{**}_{cycle} \tag{2.7}$$

$$< M >_{rem} = < M >_{remmax}, \qquad H_{cycle} > H^{**}_{cycle} \tag{2.8}$$

In our setup, the evolution of $< B >$, hence $< M >$ are continuously monitored as H_a is impressed and removed. In our arrangement this is accomplished using a pickup coil which embraces the sample and feeds an electronic amplifier-integrator which drives the Y axis of an XY recorder. The X axis is driven by a voltage across a calibrated shunt traversed by the current I flowing in the solenoid which generates H_a.

We recall the basic relationship between $< B >$ and $< M >$, namely,

$$< B >= \mu_0 H + \mu_0 < M > \tag{2.9}$$

where $\mu_0 = 4\pi(10^{-7})$ Tesla-meter/ampere in S.I.units. Clearly when $H_a = 0, < B > = \mu_0 < M >$. In our setup, we monitor $< M >$ directly by introducing a balancing (bucking) coil series opposition connected to the main pickup coil. This balancing pickup coil cancels out the contribution to the signal caused by the applied magnetic flux

$$\Phi_a = \mu_0 H_a A \tag{2.10}$$

where A is the cross section of the sample.

In the discussion it is sometimes easier to consider $< B >$ rather than $< M >$. We will consequently 'switch' the focus between these two related quantities depending on convenience.

The evolution of $< B >$ as H_a is impressed and removed can readily be analyzed in terms of the elements already introduced. By definition,

$$< B >= \frac{1}{X} \int_0^X B(x)dx \tag{2.11}$$

for planar geometry and

$$< B >= \frac{2}{R^2} \int_0^R B(r)rdr \tag{2.12}$$

for cylindrical geometry where H_a hence B(r) are directed along the axis of the infinite cylinder of radius R.

Again we refer the reader to Fig.2.1. If no discontinuity exists in the B profile,integration

of the critical state eqn. $dB/dx = \mu_0 j_c$ leads to

$$B(x) = \mu_0 \int_{x_p}^{x} j_c(x)dx \tag{2.13}$$

If a discontinuity is postulated,

$$B(x) = f B_{c1} + \mu_0 \int_{x_p}^{x} j_c(x)dx \tag{2.14}$$

In the case of cylindrical geometry, the radius r replaces the coordinate x in equations (2.13 and 2.14). The boundary x_p of penetration of the B profile goes to zero when $B_s = B_*$.

The critical current density j_c generally depends on B, hence $j_c(x)$ will usually not be spatially uniform since B varies with depth inside the sample.

A quantitative analysis of the locus of $< B >$ vs H_a therefore requires the following ingredients or inputs:

(i) the magnitude of the discontinuity fB_{c1},

(ii) the dependence of j_c on B and

(iii) the relationship between B_s, the magnetic flux density just inside the surface of the specimen and $\mu_0 H_a$, the applied magnetic flux density just outside the surface. This relationship can be written,

$$B_s = \mu_0(H_a - I_M - I_b) \tag{2.15}$$

Here I_M denotes the equilibrium diamagnetic current per unit length when H_a exceeds H_{c1} and I_b,the current per unit length associated with a surface barrier ΔH_{en} opposing

entry of magnetic flux across the surface. We note that both I_M and I_b are sensitive to the magnitude of H_a. Here $I_M = M_{rev}$, which is the well established Abrikosov [1] reversible magnetization curve.

Clearly then, in view of all these factors and complications, it is very difficult to extract unambiguous information regarding the presence of a discontinuity from curves of $< B >$ (or $< M >$) as H_a is impressed and removed.

Plots of $< B >_{rem}$, hence $< M >_{rem}$ versus H_{cycle} such as displayed in Fig.2.4(a) suffer from the same ambiguities and problems of interpretation as the rising and descending data curves just mentioned. Although now only (i) and (ii) listed above come into play in governing $< M >_{rem}$; the latter quantity is plotted in terms of the experimental variable H_{cycle}. We note however, that the excursion of the B profile is not 'directly' related to H_{cycle} but is effectively dictated by B just inside the surface, i.e. B_s. The reader is again referred to Fig.1 for assistance in following this feature. B_s is linked to $H_a = H_{cycle}$ via equation (2.15), which contains two quantities, I_M and I_b. Both of these quantities are functions of H_a and must be determined or estimated in order that B_s be completely specified for a given H_a.

In order to circumvent this problem we have proposed an alternative approach which we now describe.

2-2-2 Our Method: $< M >_{rem}$ vs $< B >_{in}$

We avoid introducing H_{cycle}, hence $I_M(H_a)$ and $\Delta H_{en}(H_a)$ in the analysis by focusing on $< B >_{in}$, the magnetic flux density permeating the specimen when $H_a = H_{cycle}$. We stress that $< B >_{in}$, mathematically defined by equations 2.11 and 2.12, is a readily measured quantity (see Fig.2.1) and note that each $< B >_{rem} = \mu_0 < M >_{rem}$ is directly linked to a corresponding $< B >_{in}$ as illustrated in Fig.2.3(a).

For each B(x) profile, hence each $< B >_{in}$ established when $H_a = H_{cycle}$, there is a corresponding B(x) profile after H_a has been removed. In Fig.2.5 we display these profiles for the situation where no discontinuity is envisaged in the B profiles and for the case where a discontinuity fB_{c1} is postulated.

We have developed analytic formulae for both $< M >_{rem}$ and $< B >_{in}$ for both of these scenarios for a variety of circumstances which we list here:

(i) Planar (slab) and cylindrical geometry ;

(ii) Three 'standard' dependences of the critical current density on B, namely,

(a) the Bean approximation where,

$$j_c = \alpha_B \tag{2.16}$$

(b) the 'Yasukochi' approximation [30, 31] where,

$$j_c = \frac{\alpha_Y}{B^{1/2}} \tag{2.17}$$

(c) the simple Kim approximation where,

$$j_c = \frac{\alpha_K}{B} \tag{2.18}$$

and,

(d) the general Kim approximation where,

$$j_c = \frac{\alpha_K}{B + B_0} \tag{2.19}$$

where α_B,α_Y,α_K and B_0 are temperature dependent parameters characterizing the pinning behaviour of the specimen.

These four well known approximations can readily be obtained from the general expression,

$$j_c = \frac{\alpha}{(B + B_0)^n} \tag{2.20}$$

(iii) Discontinuities fB_{c1} of various magnitudes where f ranges from 0 to 1.0.

The formulae for $< B >_{rem} = \mu_0 < M >_{rem}$ and $< B >_{in}$ are developed and presented in Appendix A for the general expression (eqn.2.20) for j_c, hence contain the specific instances (Bean, Yasukochi, Kim) enumerated above.

The experimental arrangement and procedure is outlined in the next chapter. The experimental results are presented and discussed in chapter 4 where they are also compared with predictions of the model with and without a discontinuity in the B profile.

2-2-3 Field Cooled (FC) procedure

For completeness, we close this chapter with a description of the field cooled (FC) procedure for generating a remanent magnetic moment. The reader is referred to Fig.2.2(b) which displays the path followed in the H-T plane.

When the temperature crosses the H_{c2}-T_c boundary, the magnetic flux permeating the specimen becomes quantized and adopts a discrete structure of flux vortices or flux lines. Because of their mutual repulsion, some of the flux lines are expelled until an equilibrium is reached where the flux line density, $B = B_{eq}$,is in equilibrium with the magnetic 'pressure' associated with $H_a = H_{cool}$. The difference between $\mu_0 H_{cool}$ and B_{eq} corresponds to the famous Abrikosov [1] curve for the reversible diamagnetism,M_{rev}, of type II superconductors, where,

$$\mu_0 M_{rev} = B_{eq} - \mu_0 H_a \tag{2.21}$$

We stress that by Ampere's eqn., this corresponds to a diamagnetic (screening or flux expelling) surface current, denoted I_M, where,

$$\mu_0 I_M = B_{eq} - \mu_0 H_a \tag{2.22}$$

When $H_a = H'_{cool} < H_{c1}$, and there is no pinning or surface barrier, the flux lines completely expel each other out of the specimen as the H_{c1}-T_c boundary is traversed. Thus here $B_{eq} = 0$, and $I_M = H_a$. We refer the reader to Fig.2.6(c) and (d) which displays various

profiles generated by field cooling in $H_{cool} = H'_{cool} < H_{c1}$ and Fig.2.6(a) and (b) for the case where, $H_{c1} < H_{cool} = H''_{cool} < H_{c2}$.

In reversible, i.e. pinning free materials, the magnetic flux density is uniform on the quasi-macroscopic scale embracing the cross section of several vortices. Hence, $B(x) = B_{eq}$. The self expulsion of flux lines by their mutual repulsion, however, may be opposed by pinning. Consequently, the B profiles resulting from field cooling are not uniform but develop configurations such as sketched in Fig.2.6. The final configurations are traced on the left hand figures when the pinning is weak and on the right hand side when the pinning is strong. We also stress that , when H_{cool} is still present, the B(x) profiles will, generally, be in a critical state only in the vicinity of the surface and only when $H_{cool} = H''_{cool} > H_{c1}$ [16].

The B(x) profile remains unchanged when H_{cool} is removed for the case where $H_{cool} = H'_{cool} < H_{c1}$ (see Fig.2.6(c) and (d)). B(x) profiles such as indicated by the dashed lines in Fig.2.6(a) and (b) will ensue when H_{cool} is removed where initially $H_{cool} = H''_{cool} > H_{c1}$. We note that in all of these situations the discontinuity fB_{c1} in the B profile plays no role in the remanent magnetization.

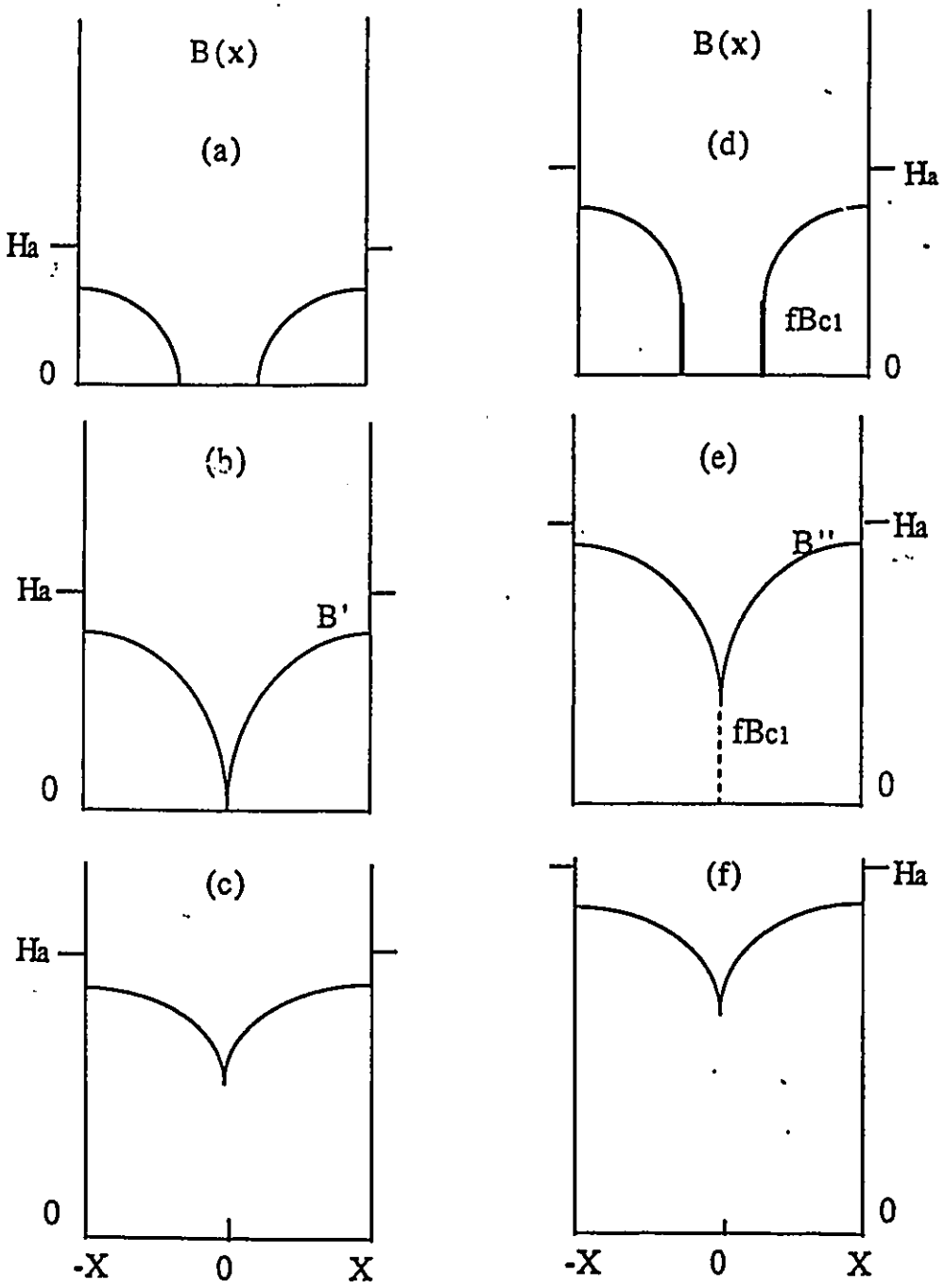

Figure 2.1: B profiles without discontinuity (on the left) and with discontinuity (on the right) as the magnetic flux enters a specimen

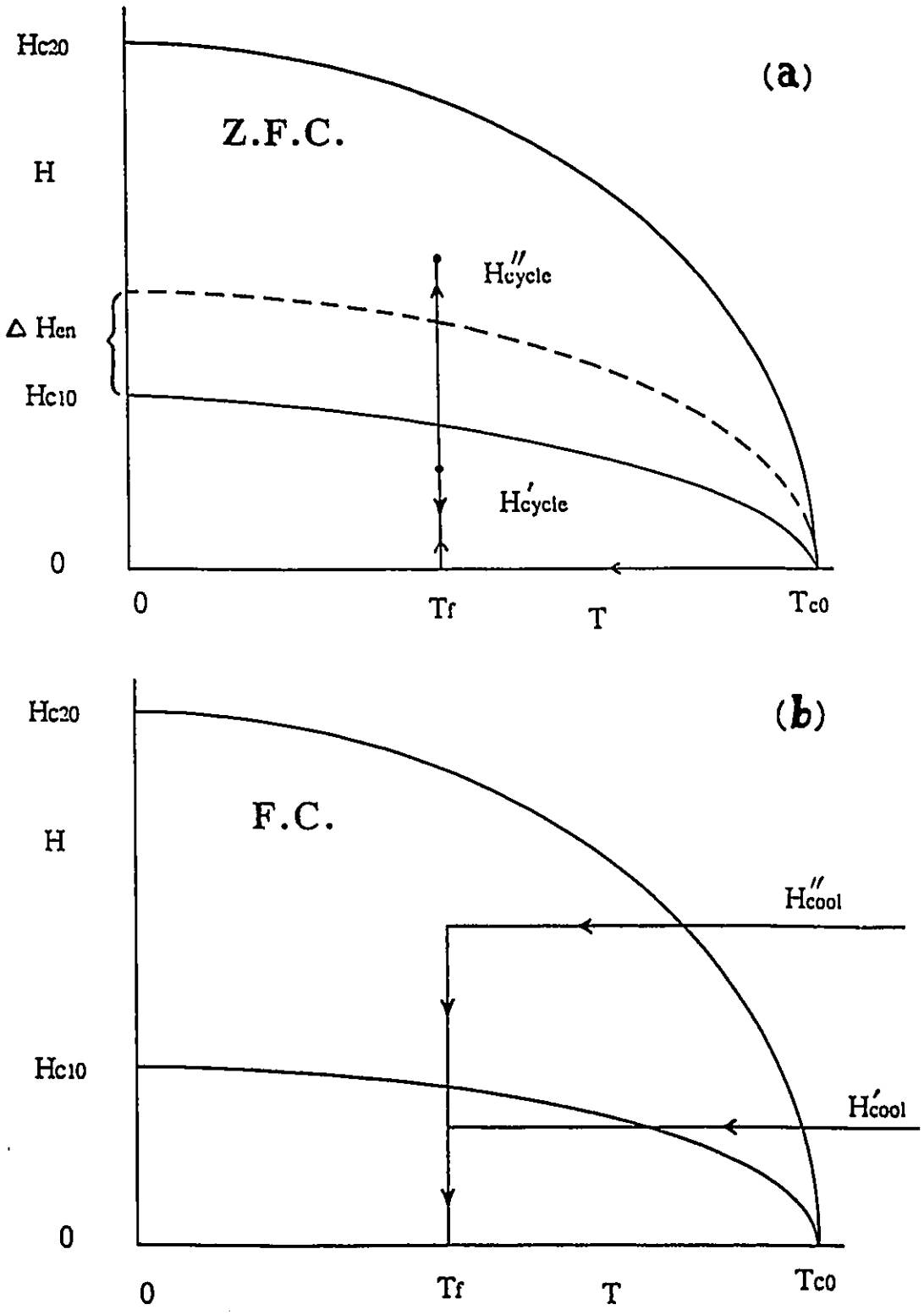

Figure 2.2: Schematic of the history traversed by H and T when a remanent magnetic moment is established using the zero field cooled (Z.F.C.) and field cooled (F.C.) procedures

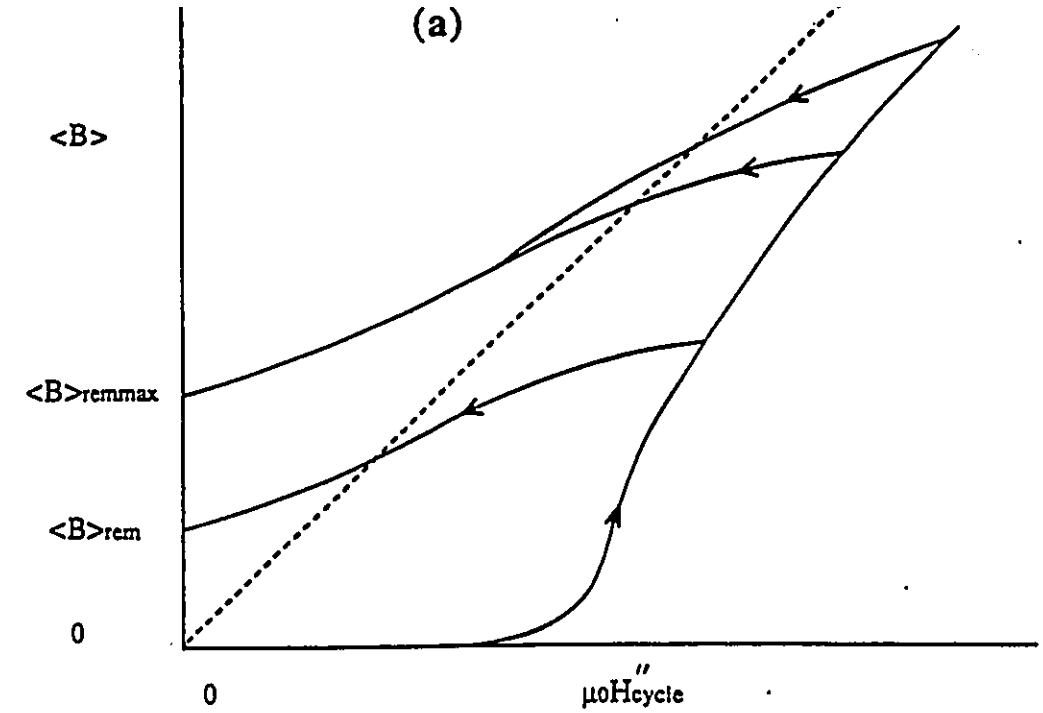

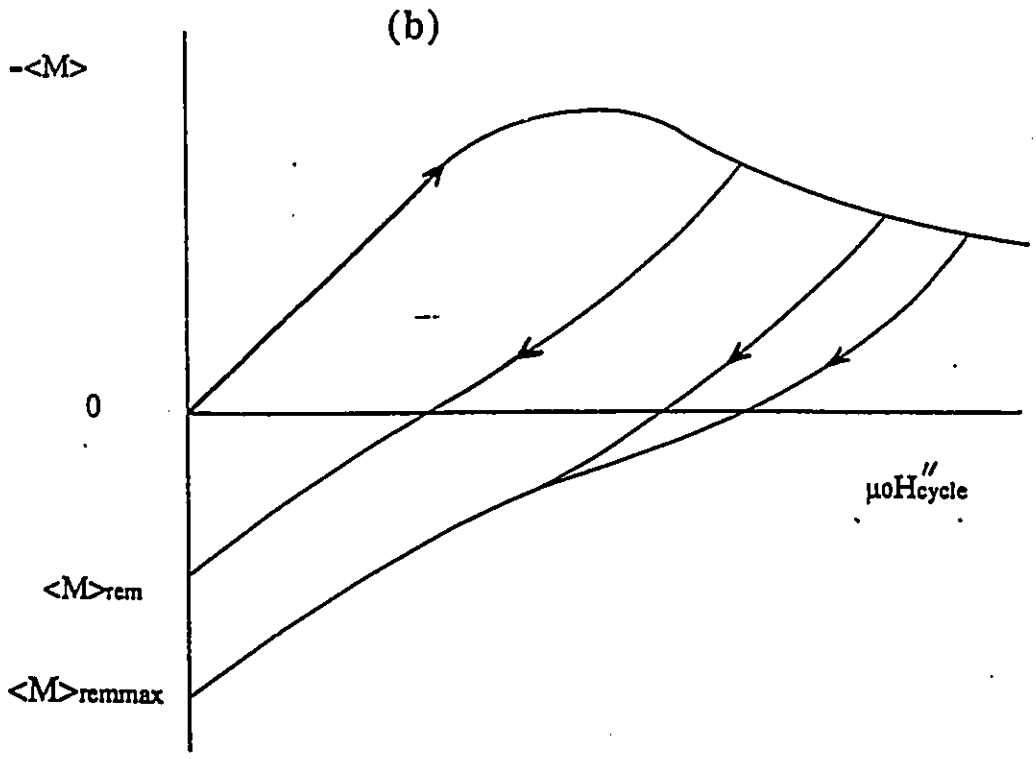

Figure 2.3: Evolution, (a) of the magnetic flux density $< B >$ and, (b) of the magnetization $< M >$ as the magnetic field is applied to various values after zero field cooling and then removed

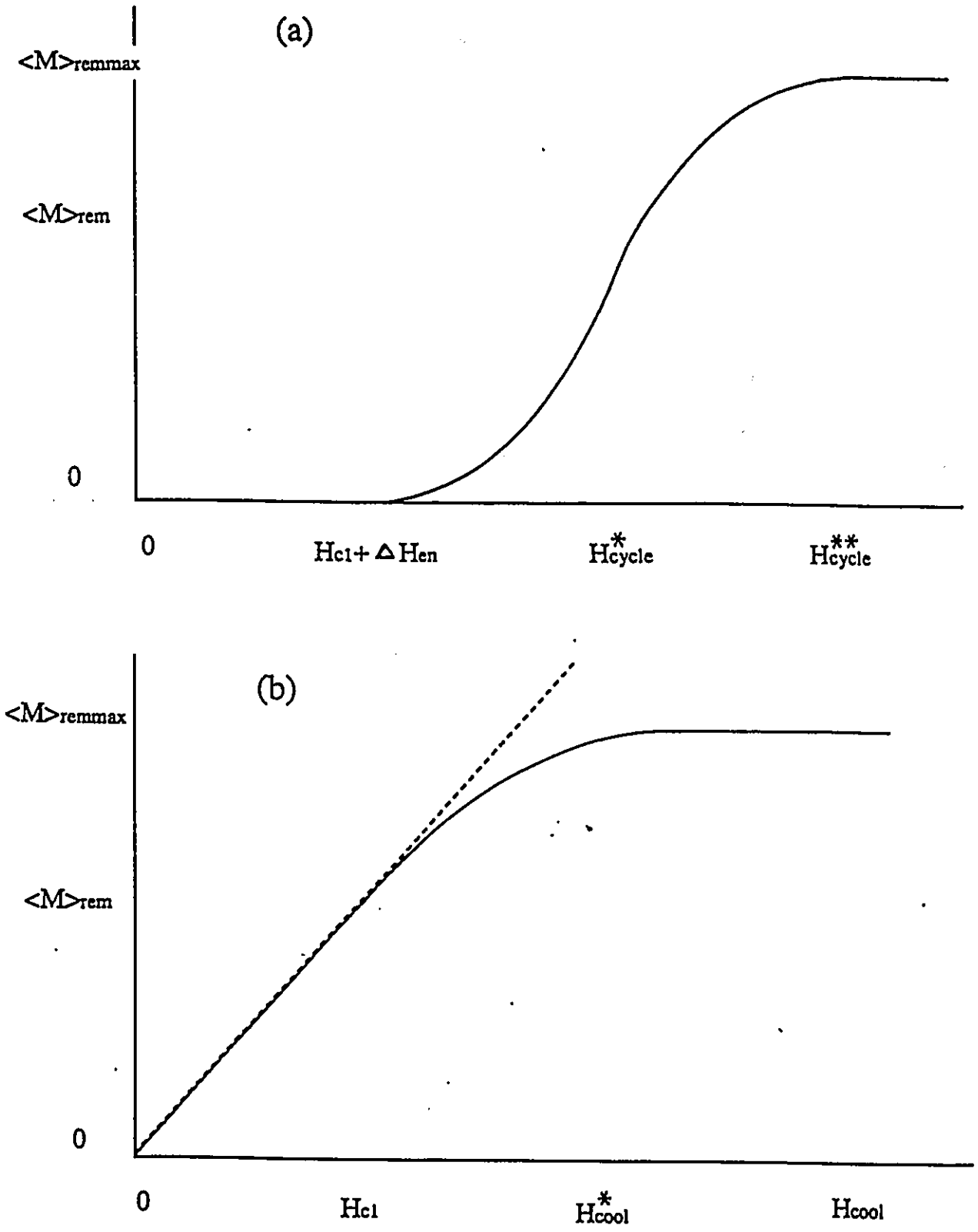

Figure 2.4: Schematic of expected and observed evolution of $< M >_{rem}$ versus H_{cycle} and H_{cool}

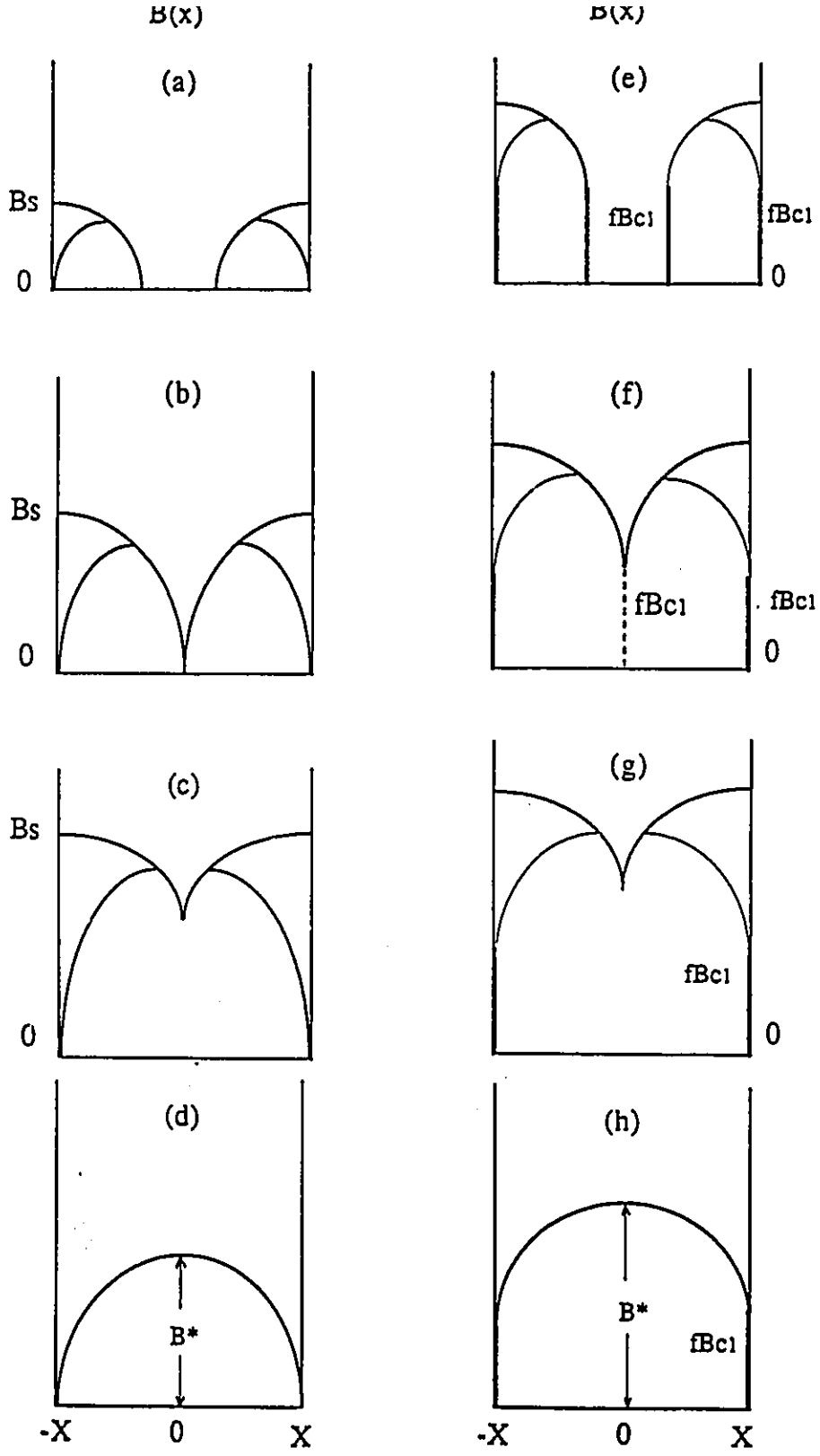

Figure 2.5: The initial and remanent B profiles as H_{cycle} hence B_s is applied and removed. The configurations without a discontinuity are sketched on the left and with a discontinuity on the right

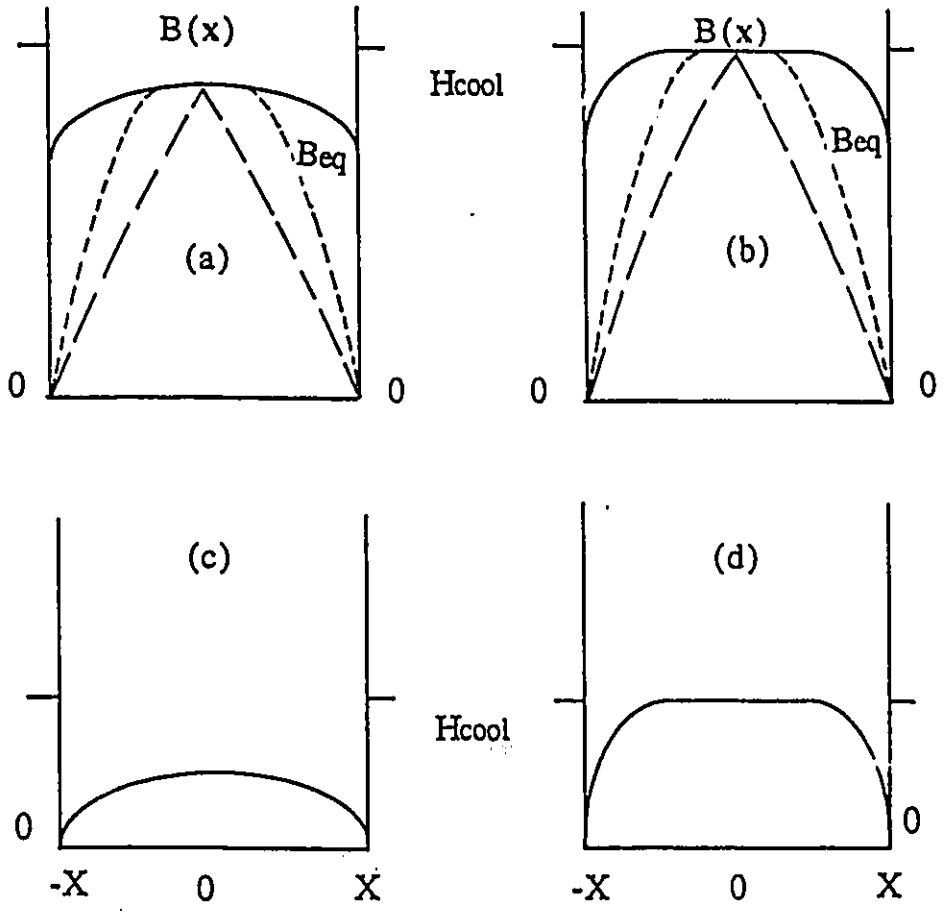

Figure 2.6: Solid curves display B profiles after field cooling. $H_{cool} > H_{c1}\ (T_f)$ for (a) and (b) whereas $H_{cool} < H_{c1}\ (T_f)$ for (c) and (d). The pinning is weak in (a) and (c) compared to that envisaged in (b) and (d). The dashed lines represent the remanent B profiles for the cases where $H_{cool} < H_*$ (lower profiles) and where $H_{cool} > H_*$ (upper profiles)

Chapter 3

Experimental Arrangement and Procedure

3-1 Introduction

Measurements have been performed on long cylinders (wires) and ribbons or slabs of several 'classical' (low T_c) type II superconductors. Because of 'internal' demagnetization effects, the determination of $< B >_{in}$ and $< M >_{rem}$ is very ambiguous for sintered high-T_c samples we have obtained to date. These yield data inappropriate for the present study. We expect to obtain satisfactory samples in the near future and it is intended to extend this investigation to these materials at that time.

3-2 Magnetic Field H_a

The magnetic fields were provided by various long superconducting solenoids wound with multifilamentary NbTi wire. Typically, the dimensions of the solenoids were as follows: 15 cm length, 4.5 cm outer diameter and 2.5 cm inner diameter. The residual magnetic field of these solenoids is negligible, especially over the low range of H_{cycle} involved in these measurements.

A standard calibrated shunt of resistance R_s is placed in the circuit of the power supply and superconducting solenoid and hence is traversed by the current I flowing in the solenoid. The voltage $V_s = IR_s$ drives the X axis of an XY recorder. The magnetic field H_a at the center of the solenoid is obtained from the law of Biot-Savart,

$$\Delta\vec{B} = \frac{\mu_0}{4\pi}\frac{\vec{j}\times\vec{R}}{R^3}dv \tag{3.1}$$

which leads to,

$$B = \mu_0 H_a = \frac{\mu_0 NI}{2(R_0 - R_i)} ln[\frac{{R_0}^2 + \sqrt{{R_0}^2 + (L/2)^2}}{{R_i}^2 + \sqrt{{R_i}^2 + (L/2)^2}}] \tag{3.2}$$

where N is the total number of turns, L is the length of the solenoid in meters and R_i,R_0 are the inner and outer radius of the solenoid winding in meters.

3-3 Sample Arrangement

A noninductive (bifilar) single layer heater coil of 38 B&S manganin wire is wound on the sample holder. The advantages of the manganin is that, (i) it is nonmagnetic and, (ii) its resistivity is large. In view of the latter, only a small current is required to cause sufficient joule (I^2R) heating to raise the temperature of the sample above T_c. The small heater current and noninductive bifilar winding ensure that the heater coil generates no flux. This is important since $< B >_{rem}$ is measured by heating the sample from T_f to above T_c. Any flux generated by the heater would then contribute to $< B >_{rem}$. We verify that the heater generates no flux by driving a large current through it with the sample in the normal state or no sample present.

The sample holder is rigidly positioned at the center of the solenoid and embraced by a main pickup coil series opposition connected to a pair of bucking coils placed symmetrically one above and one below the main coil. These bucking coils do not embrace the sample but are threaded by the magnetic field H_a. The area turn product of the pair of bucking coils is carefully adjusted so that the emf they generate when H_a is changed, cancels that of the empty main coil (or with the sample in the normal state). This scheme therefore monitors $< M >$, the spatial average of the magnetization of the sample.

3-4 Measurement of $< M >$ vs H_a and $< M >_{rem}$

The emf ε from the pickup coil system is fed to an integrator-amplifier. Consequently a change of the magnetization $\Delta < M >$ caused by an increment or decrement ΔH_a is detected since the signal S from the integrator reads,

$$S = c\int_{t_1}^{t_2} \varepsilon dt = c\int_{t_1}^{t_2} A\frac{d < M >}{dt}dt = cA\Delta < M > \tag{3.3}$$

where $\Delta t = t_2 - t_1$ and c is the amplification factor.

We recall that $< B >= \mu_0 H_a + \mu_0 < M >$ and that the bucking coil cancels out any contribution arising from ΔH_a.

The signal S drives the Y axis of an XY recorder. With this arrangement we can continuously monitor and record the evolution of $< M >$ as H_a is cycled from 0 to H_{cycle} and back to zero.(see figure 2.3(b)). The signal due to any residual imbalance of the pickup coil system is determined by applying H_a with the sample in the normal state. The detecting system is calibrated on the standard assumption that the persistent currents induced at the surface of the specimen completely screen its volume from entry of H_a when $H_a < H_{c1}$, hence here $< B >= 0$.

After an excursion of H_a (ie.H_{cycle}), with H_a now zero, the temperature of the sample is raised to T_c by means of the manganin wire heater. The rise in temperature and onset of the normal state causes the persistent circulating currents sustaining the trapped flux

to decay rapidly, thereby releasing the latter and causing the remanent magnetic moment to collapse. The corresponding signal detected by the pickup coil and registered on the Y axis of the XY recorder, provides a direct and unambiguous measure of $< M >_{rem}$. We stress that this measurement is not affected by any electronic drift or stray signals which may have occurred during the 'half' cycle of H_a from 0 to H_{cycle} and back to zero.

In our set-up, it is also straightforward to measure $< B >_{in}$, or the corresponding $< M >$ 'directly' by driving the sample normal using the manganin wire heater to raise its temperature to T_c with H_a held stationary at H_{cycle}.

3-5 Experimental Procedure

The specimen is first allowed to cool from above T_c to the ambient temperature $T_f < T_c$ in zero applied magnetic field (the earth's field). In our work $T_f = 4.2K$, the temperature of liquid helium at atmospheric pressure (see figure 2.2(a)). H_a is then applied, slowly to a pre-selected value, denoted as H_{cycle}' when below H_{c1} (or $H_{c1} + \Delta H_{en}$) and H_{cycle}'' when above H_{c1} (or $H_{c1} + \Delta H_{en}$). We stress that H_{cycle} , hence $H_{c1} + \Delta H_{en}$, does not enter in our analysis of the data. For completeness, however, we note that $H_{c1} + \Delta H_{en}$ is determined by the onset of entry of magnetic flux into the sample. In our work, this is identified by,(i) the appearance of a deviation from a straight line along the initial part of the $< M >$ or $< B >$ vs H_a curve, or (ii) the onset of a remanent magnetic moment after H_a is removed.

After having maintained H_a at its maximum value H_{cycle}, for a few seconds, the magnetic field is reduced to zero gradually. The sample is then heated above T_c, providing a 'final' determination of $\mu_0 < M >_{rem} = < B >_{rem}$. In the absence of electronic drift during the excursion of H_a, the locus of $< M >$ vs H_a (or $< B >$ vs H_a) traces a curve which is closed. We stress that in our work, it was not necessary that this requirement be met. Nevertheless, all curves which display significant deviation from closure were rejected.

The imbalance of the pickup coil system is determined by applying H_a with the sample held in the normal state by energizing the manganin wire heater. The curves of $< M >$ vs H_a (or $< B >$ vs H_a) are corrected for this background. This is a straightforward matter, since in our work this background signal is small and linear with H_a.

3-6 Samples

We report on measurements performed on solid cylinders several centimeters long (typically $\approx$4 cm) with the radius indicated in parentheses:

Nb_3Zr	(0.0125 cm)
$Nb_{0.5}Ta_{0.5}$	(0.0625 cm)
$Pb_{0.86}In_{0.14}$	(0.0625 cm)
$Pb_{0.45}Bi_{0.55}$	(0.25 cm)
V	(0.0625 cm)

and on a ribbon of pure Nb, 4 cm long, 1 cm wide and 0.025 cm thick.

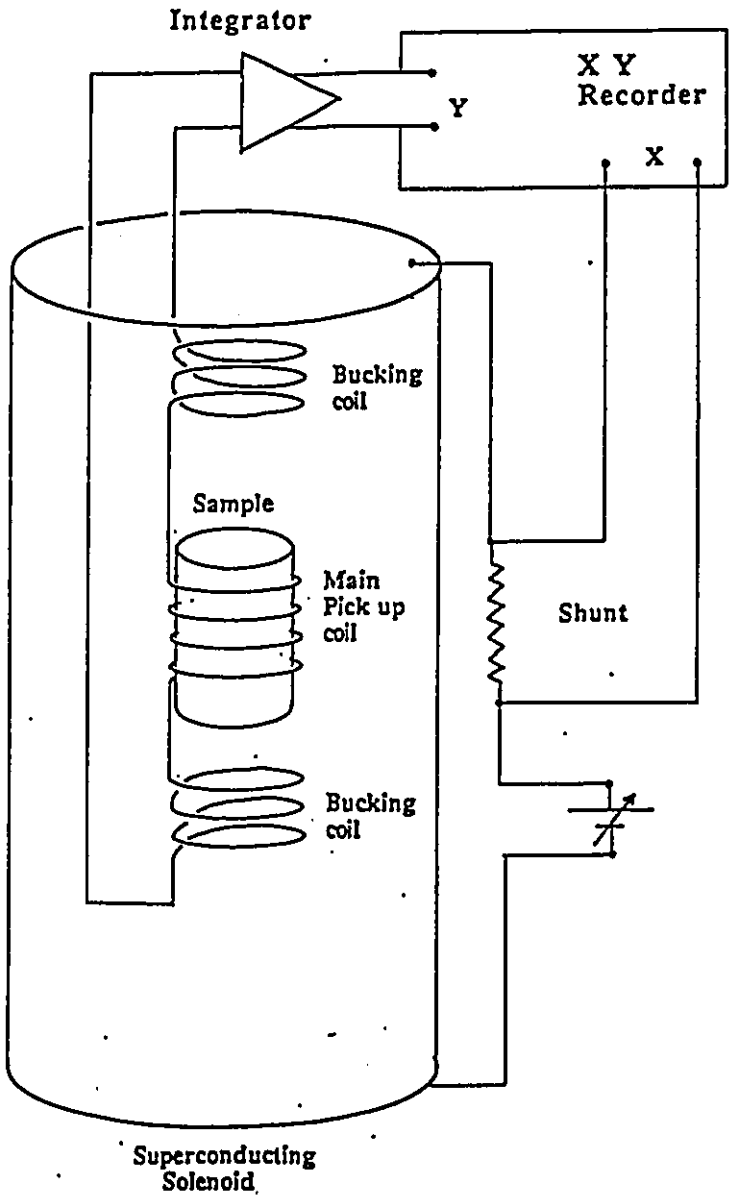

Figure 3.1: Block diagram of experimental arrangement

Chapter 4

Results and Discussion

4-1 Introduction

In this chapter we first present the predictions of the CSM ('critical state model') for the behaviour of $< M >_{rem}$ versus $< B >_{in}$ both with and without a discontinuity in the B profile. Then we compare these predictions with observations on several classical type II superconductors of two different geometries.

4-2 Framework of the Analysis

We explore the predicted effect of a discontinuity and its absence in samples of two idealized geometries: planar (infinite slab) and cylindrical. A variety of analytic functions have been

exploited in the literature to describe the dependence of the critical current density j_c on the magnetic flux density in different materials. Two simple expressions conveniently bracket the spectrum of behaviour. These are denoted as the Bean and simple Kim approximations. The former simply stipulates that j_c is independent of B. Hence here the B profiles are constructed with straight lines of constant slope, since Maxwell's equation, $\nabla \times \vec{B} = \mu_0 \vec{j}$ reads,

$$\frac{dB}{dr} = \frac{dB}{dx} = \pm \mu_0 j_c = \pm \mu_0 \alpha_B \tag{4.1}$$

where α_B is a temperature dependent parameter characterizing the specimen. The simple Kim approximation assumes that j_c is inversely proportional to B hence, the critical state equation reads,

$$\frac{dB}{dr} = \frac{dB}{dx} = \pm \mu_0 j_c = \pm \frac{\mu_0 \alpha_K}{B} \tag{4.2}$$

where α_K is also a temperature dependent parameter characterizing the specimen. Actually, Kim and co-workers first introduced a more realistic two-parameter expression of the form,

$$j_c = \frac{\alpha_K}{B + B_0} \tag{4.3}$$

where B_0 is another parameter (dependent on temperature) characterizing the specimen. Evidently, if B_0 is large compared with the range of B under scrutiny, hence dominates B, eqn.(4.3) becomes equivalent to eqn.(4.1) (the Bean approximation). We will also examine the effect of varying B_0 on the behaviour of $< B >_{rem}$ vs $< B >_{in}$ since the various

choices of B_0 lead to behaviour spanning the range between the 'extremes' or 'boundaries' represented by eqns. (4.1) and (4.2).

It is of interest to note that the spectrum of behaviour lying between the limits set by the Bean and Kim approximations (eqns. 4.1 and 4.2) can be scanned by writing the dependence of the critical current density in the form,

$$j_c = \frac{\alpha}{B^n} \tag{4.4}$$

where $0 \leq n \leq 1$.

Historically, Yasukochi et al[30, 31] were the first to demonstrate that the behaviour of a large variety of the materials over an appreciable range of B could be described by taking $n = 1/2$. Consequently, we have also examined this form for j_c, namely,

$$j_c = \frac{\alpha\gamma}{B^{1/2}} \tag{4.5}$$

and refer to this as the Yasukochi approximation. As expected, this expression generates behaviour intermediate between the Bean and simple Kim formulae (eqns. 4.1 and 4.2).

4-3 Theoretical Predictions

The development of the critical state expressions for $< B >_{in}$ and $< B >_{rem}$ for two basic geometries and a generalized critical current function which encompasses the Bean,

Yasukochi and Kim approximations, namely,

$$j_c = \frac{\alpha}{(B + B_0)^n} \tag{4.6}$$

is presented in appendix A. The various final formulae for these quantities are also tabulated in that appendix. These equations communicate analytically and quantitatively, the physical scenario illustrated in Fig.2.5.

It is most useful to compare the magnitude of the discontinuity in the B profile with the full penetration field B_*. The reason is that for a chosen geometry, it is these two quantities which dictate the magnitude of the remanent magnetic moment and we wish to identify the role of the former (fB_{c1}) relative to that of the latter (B_*). Consequently, we introduce the parameter $b_1 \equiv fB_{c1}/B_*$.

It is also convenient to normalize both $< B >_{in}$ and $< B >_{rem}$ with respect to the corresponding maximum remanent magnetization $< B >_{remmax}$. This 'scaling' not only generates universal curves but also provides a very useful format for displaying the results. The reason is that $< B >_{remmax}$ is seen to trace a plateau whose height can be unambiguously and accurately measured in experiments.

Figures 4.1 through 4.4 display $< B >_{rem}$ versus $< B >_{in}$ (normalized as indicated above) for the two basic geometries (slab and cylinder) and the 'extreme' j_c functions (Bean and Kim). Each figure also illustrates the effect of an increase in the discontinuity in the B profile from zero to B_*, (ie. $b_1 = 0$ to $b_1 = 1.0$). Again all the figures are

Table 4.1: Theoretical $\frac{<B>_{inmin}}{<B>_{remmax}}$ at the edge of the plateau

$\frac{<B>_{inmin}}{<B>_{remmax}}$	Slab	Cylinder	$b_1 = fB_{c1}/B_*$
Bean	3	5	0
Bean	2	13/5	0.5
Bean	5/3	2	1.0
Bean	3/2	19/11	1.5
Kim	$(2\sqrt{2}-1) \sim 1.828$	$(\sqrt{2}+1) \sim 2.414$	0
Kim	$\frac{5\sqrt{5}-3\sqrt{3}}{\frac{11}{4}\sqrt{11}-3\sqrt{3}-\frac{1}{4}\sqrt{2}} \sim 1.626$	$\frac{1+\frac{27}{25}\frac{1}{\sqrt{5}}}{1-\frac{11}{25}\frac{1}{\sqrt{5}}} \sim 1.846$	0.5
Kim	$\frac{3\sqrt{3}-2\sqrt{2}}{2\sqrt{2}-1} \sim 1.295$	$\frac{4\sqrt{2}-1.5\sqrt{3}}{4\sqrt{2}-3.5} \sim 1.418$	1.0
Kim	$\frac{7\sqrt{7}-5\sqrt{5}}{\frac{23}{4}\sqrt{23}-5\sqrt{5}-\frac{27}{4}\sqrt{2}} \sim 1.072$	$\frac{1-\frac{119}{169}\sqrt{\frac{17}{13}}}{1-\frac{513}{169}\frac{1}{\sqrt{13}}} \sim 1.230$	1.5

grouped in sequence at the end of the chapter for ease and continuity of examination and comparisons.

A glance at these four figures reveals that the predicted curves are very simple and display little structure. As expected, from Fig.2.5, the rise to a plateau is monotonic with the slope diminishing as the edge of the plateau is approached. We let $< B >_{inmin}$ denote $< B >_{in}$ at the onset or threshold of the plateau. Table 4.1 displays the theoretical values predicted for this quantity for 16 cases.

Although, in most intances, the approach to the plateau is very gradual and shallow,

Table 4.2: Experimental $\mu_0 < M >_{remmax}$ values (in millitesla)

Nb	NbTa	NbZr	PbBi	PbIn	V
95.5	49.0	$\gg$400	56.5	21.4	106.5

it is a straightforward matter to compute the theoretical values for $< B >_{inmin}$, quite exactly. This exercise merely involves introducing the appropriate theoretical limit in the analytic formulae. Experimentally, however, because of the asymptotic behaviour of the curves, the threshold is difficult to identify accurately. Consequently, in view of the large uncertainty in establishing the position of the edge of the plateau from the experimental data, this quantity does not serve as a good yardstick for assessing the presence or absence of a discontinuity in the B profiles.

The growth of $< B >_{rem}$ versus $< B >_{in}$ over their low and intermediate ranges can however be readily and fairly accurately evaluated from the experimental data and compared with theoretical predictions at the corresponding normalized values. In other words, comparison of the predicted and observed ratios $< B >_{rem} / < B >_{in}$ versus $< B >_{in}$ (normalized or not) provides a much more definitive test of the presence or absence of a discontinuity in the B profiles. This arises because the growth of $< B >_{rem}$

versus $< B >_{in}$ is steep in the low field range (denoted as regime A in appendix A) and quite sensitive to the introduction of a discontinuity in the B profiles. Consequently, we next display the theoretical predictions in the more 'discriminating' format of $< B >_{rem}$ / $< B >_{in}$ versus $< B >_{in}$ / $< B >_{remmax}$ in figures 4.5 through 4.8.The crucial feature of these four figures of theoretical curves is that the presence of a discontinuity in the B profiles, no matter how small, radically alters the behaviour. This is readily seen by comparing the various curves with the lowermost ($b_1 = 0$) one in each figure. We note that the curves with $b_1 \neq 0$ (ie. with a discontinuity in the B profile) all converge to unity in the limit where $< B >_{in}$ is small. This result is not at all mysterious and is fully expected since in that limit $< B >_{rem}$ and $< B >_{in}$ differ only slightly as can be readily seen from inspection of Fig.2.5(e).

The parameter B_0 in the 'Kim like' expressions,

$$j_c = \frac{\alpha}{(B + B_0)^n} \tag{4.7}$$

is expected to play an important role in the range where $B < B_0$ when $n > 0$ [26, 34]. The effect of this parameter is illustrated for slab and cylinder geometries in Figs 4.9 and 4.10. We note that the curves now exhibit a rise in the low range of $< B >_{in}$ when there is no discontinuity in the B profile. This occurs because the locus of $< B >_{rem}$ migrates from Bean type of behaviour when $< B >_{in}$ is small towards the simple Kim regime at large $< B >_{in}$. A comparison of the lowermost curve in Fig.4.5 with that in Fig.4.7 (slab

geometry) and of the lowermost curve in Fig.4.6 with that in Fig.4.8 (cylinder geometry) is seen to account for the occurrence of a peak in the lower curves of Figs.4.9 and 4.10. Of course, if a discontinuity is postulated in the B profiles, the curves will extrapolate to unity in the limit where $< B >_{in}$ approches zero, even when the parameter $b_0 \neq 0$.

4-4 Experimental Results and Analysis

Data for six (6) different materials are displayed in figures 4.11 through 4.16 in the format of $< B >_{rem}$ versus $< B >_{in}$ and again, for completeness, in figures 4.17 through 4.22 in the alternative scheme of $< B >_{rem} / < B >_{in}$ versus $< B >_{in}$. For convenience and 'universality', the various quantities are normalized with respect to $< B >_{remmax}$, the maximum remanent magnetization.

Firstly, we invite the reader to inspect the data displayed in the format of $< B >_{rem}$ versus $< B >_{in}$ (Figs 4.11 through 4.16) and compare these data with the families of theoretical curves for the corresponding geometry displayed in the same format in Figs 4.1 through 4.4. We stress that the object of the exercise is to determine whether a discontinuity ($b_1 > 0$) hence the dB/dH effect plays a role in the behaviour of the specimens. In our view, since the experimental and theoretical curves have essentially no structure and possess no salient features in this format, no clear message emerges from the comparison. Thus no firm conclusion can be drawn in this framework.

Nevertheless in Figs 4.11 through 4.16 we have, for completeness and by way of illustration, displayed a calculated curve for each specimen. In every case, the calculated curve is based on the stipulation that there is no dB/dH effect, ie. $b_1 = 0$. The simple function selected for j_c is indicated in the caption for each figure. For simplicity, we have limited our choice to either the Bean or the Kim approximations. In the latter case, we have also introduced a parameter b_0, selected to improve the fit between theory and experiment. Although the correspondence between the data and the theoretical curves is generally quite good, we view this agreement with reservations with respect to the existence or absence of a discontinuity in the B profiles. The reason for our caution is that equally good correspondence can also be achieved between the data and the theoretical curves by the selection of appropriate combinations of $b_1 \neq 0$ and $b_0 \neq 0$ except for the PbIn cylindrical specimen. In the latter case, the choice of a Kim like function for j_c and/or the introduction of a discontinuity causes the fit to deteriorate appreciably.

Next we invite the reader to inspect the data displayed in the format of $< B >_{rem} / < B >_{in}$ versus $< B >_{in}$ (Figs 4.17 through 4.22) and compare these data with the families of theoretical curves for the corresponding geometry displayed in the same format in Figs 4.5 through 4.8. It is also instructive to note the effect of 'transforming' the dependence of j_c on B from the simple Kim approximation towards the Bean approximation illustrated in Figs 4.9 and 4.10 with and without a discontinuity.

The crucial features which emerge from this survey are that the theoretical curves presented in the format of $< B >_{rem} / < B >_{in}$ vs $< B >_{in}$, (a) exhibit structures and magnitudes which are sensitive to the dependence of j_c on B, and, (b) display a steep rise to unity in the low range of $< B >_{in}$ if a discontinuity, hence a dB/dH effect, no matter how small is postulated to exist. By contrast however, none of the experimental data curves display any hint of such a rise in the low range $< B >_{in}$. Indeed, on the contrary, some of the specimens show a downward trend in this range.

The solid curves traced in each of Figs 4.17 through 4.22 corresponds to that presented previously in the alternative format and is calculated in each case using the j_c dependence on B and parameter B_0 chosen earlier. The correspondence between the theoretical curves and the data points is now less satisfactory. This is not surprising since the format exploited here is appreciably more sensitive to the ingredients introduced in the analysis. Now in order to achieve good agreement between calculations and experiment, greater care and effort need to be exercised in the choice of dependence of j_c on B. Hence simple appproximate analytic functions of the form exploited in our work are shown to be inadequate as expected from the larger variations caused by small changes of parameters exhibited by the theoretical curves of Figs 4.5 through 4.10.

The central purpose of our investigation was not to extract the best expression for the dependence of j_c on B in the low field range but to establish whether the stipulation of

a discontinuity is correct, ie. whether the dB/dH effect is 'real'. We conclude from our measurements and our analysis that our six samples provide no corroboration for such a concept. We stress that the introduction of a discontinuity in the B profiles does not improve but exacerbates the agreement between theoretical curves and the experimental data.

4-5 Conclusion

It is not our purpose in this project to identify formulae for j_c and parameters for each specimen which lead to an optimum fit to the corresponding data. Our central object is to determine whether the data carries the signature of a discontinuity in the B profiles. Figs 4.5 through 4.8 reveal that such a discontinuity, however small, would manifest itself by a rise in $< B >_{rem}$ in the range of small $< B >_{in}$ independently of the specific choice for j_c. For all of the specimen we have investigated the trend of the data points in the range of small $< B >_{in}$ is opposite to the behaviour anticipated from the presence of a discontinuity in the B profiles.

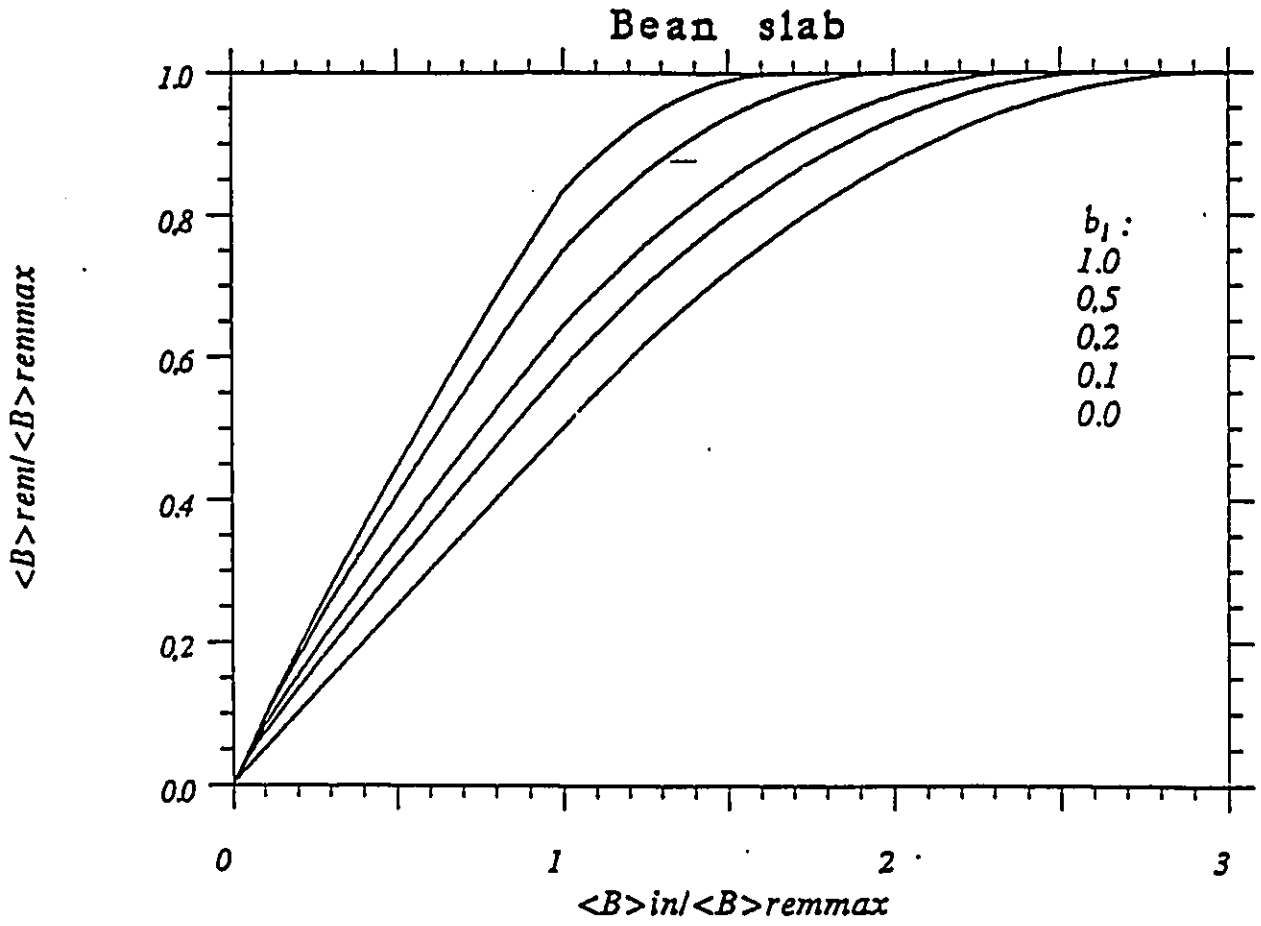

Figure 4.1: $< B >_{rem} / < B >_{remmax}$ vs $< B >_{in} / < B >_{remmax}$ for Bean slab with $b_1 = fB_{c1}/B_*$ varying from 1 to 0 from upper to lowermost curve

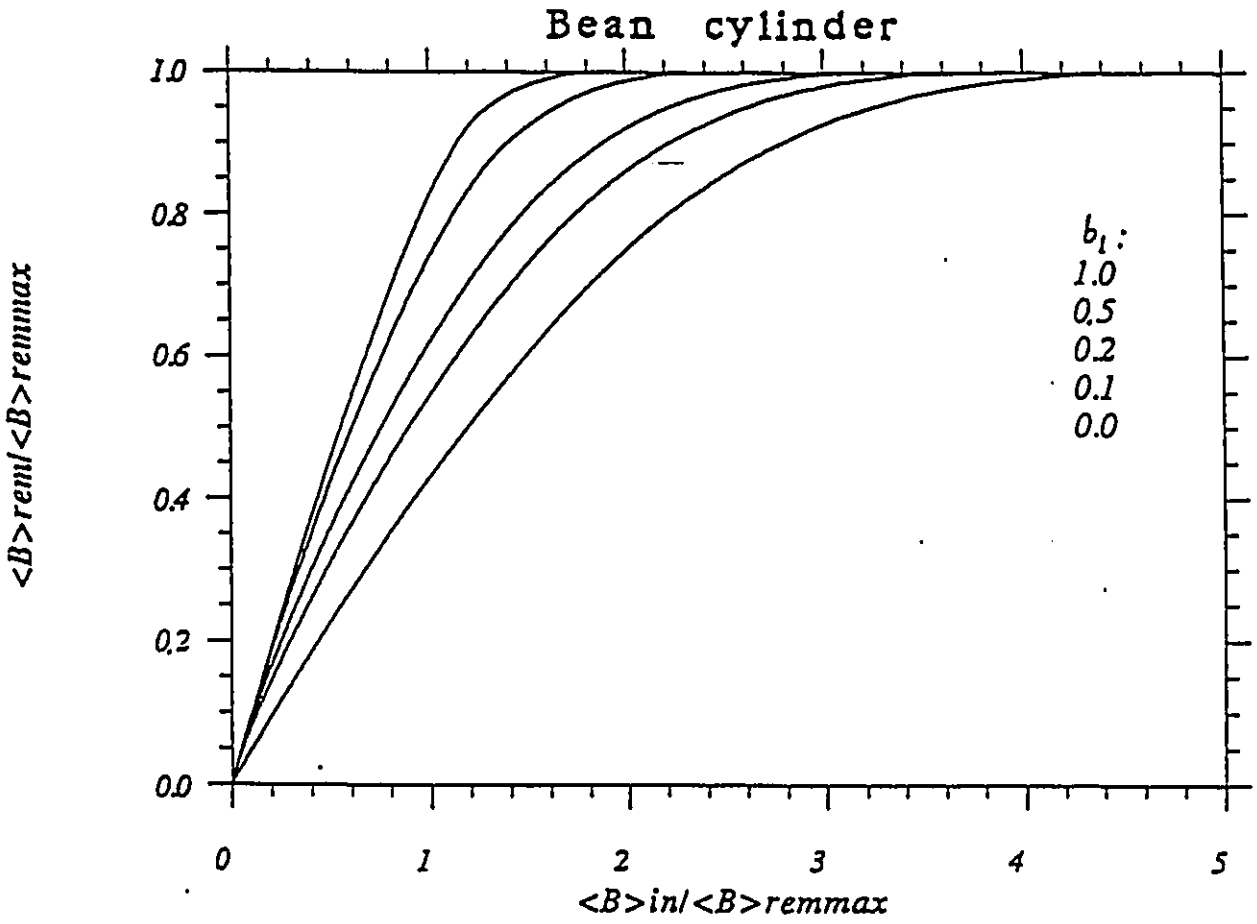

Figure 4.2: $< B >_{rem} / < B >_{remmax}$ vs $< B >_{in} / < B >_{remmax}$ for Bean cylinder with $b_1 = fB_{c1}/B_*$ varying from 1 to 0 from upper to lowermost curve

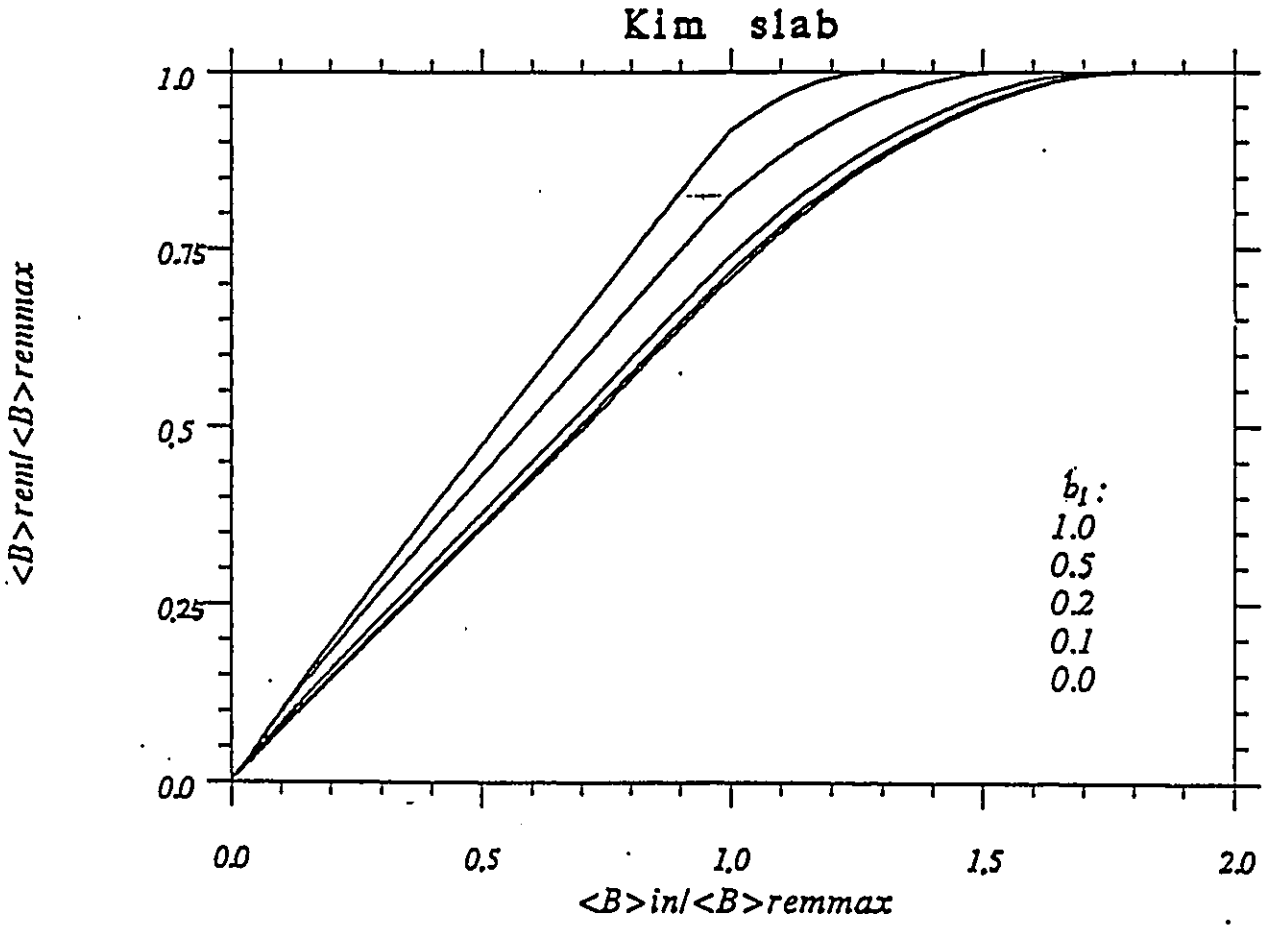

Figure 4.3: $< B >_{rem} / < B >_{remmax}$ vs $< B >_{in} / < B >_{remmax}$ for Kim slab with $b_1 = fB_{c1}/B_s$ varying from 1 to 0 from upper to lowermost curve

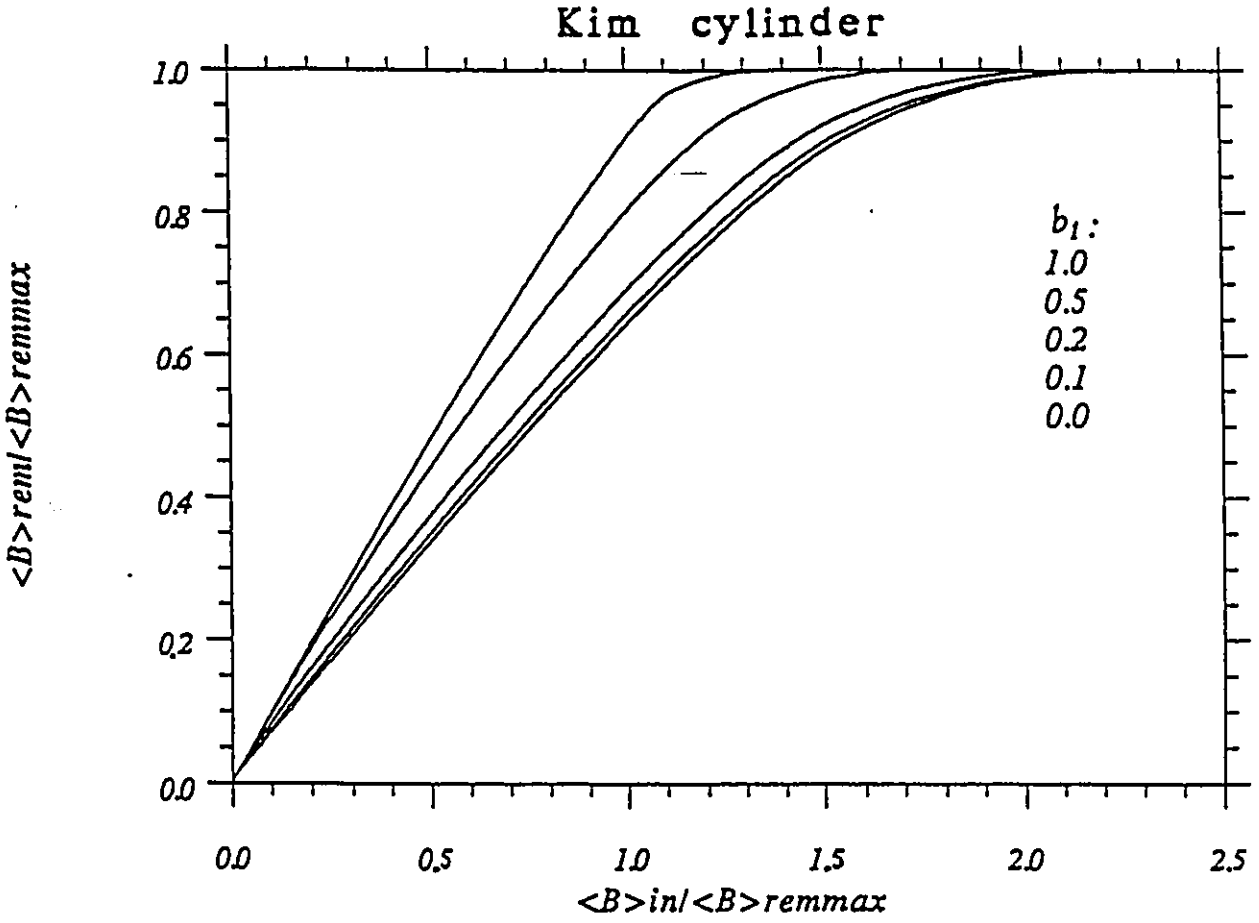

Figure 4.4: $< B >_{rem} / < B >_{remmax}$ vs $< B >_{in} / < B >_{remmax}$ for Kim cylinder with $b_1 = fB_{c1}/B_s$ varying from 1 to 0 from upper to lowermost curve

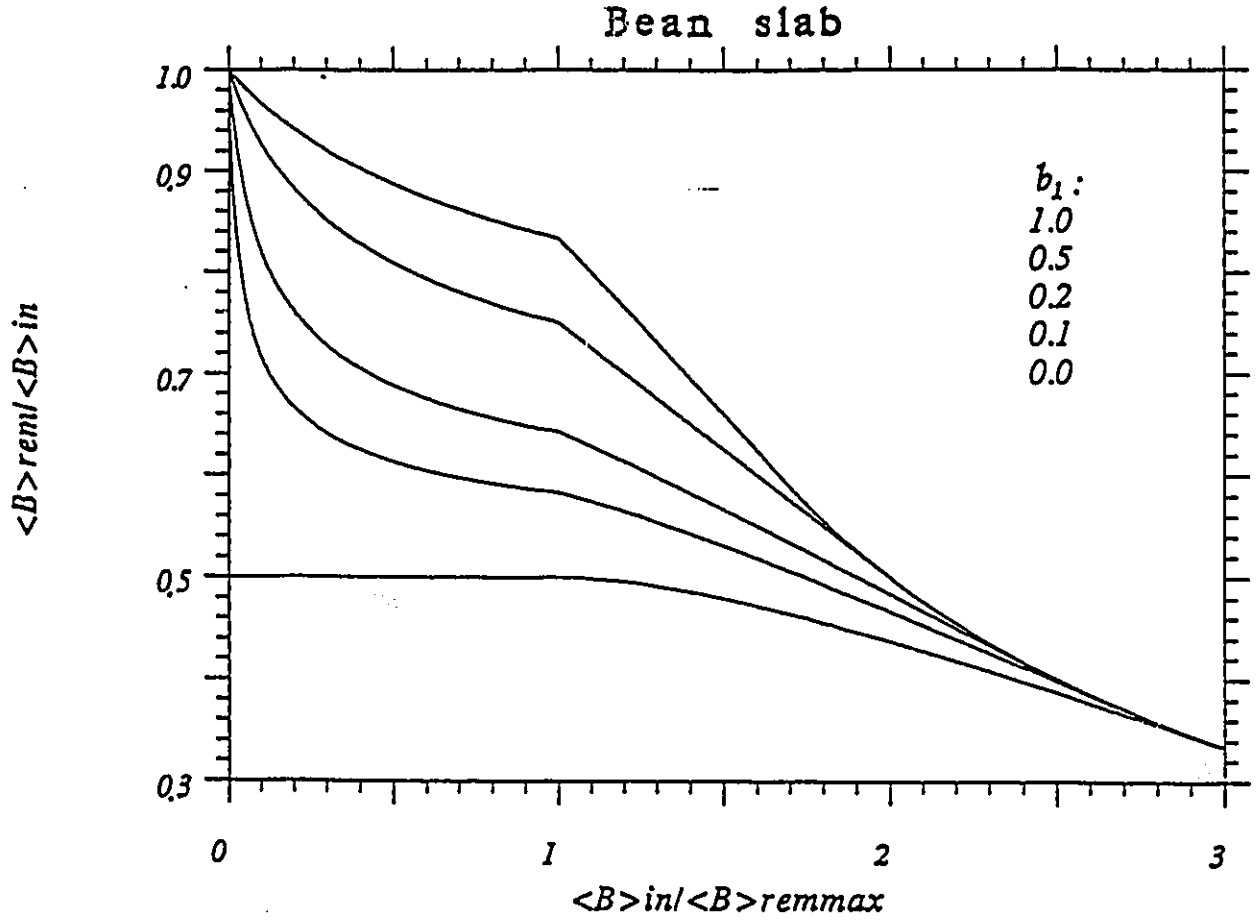

Figure 4.5: $< B >_{rem} / < B >_{in}$ vs $< B >_{in} / < B >_{remmax}$ for Bean slab with $b_1 = fB_{c1}/B_*$ varying from 1 to 0 from upper to lowermost curve

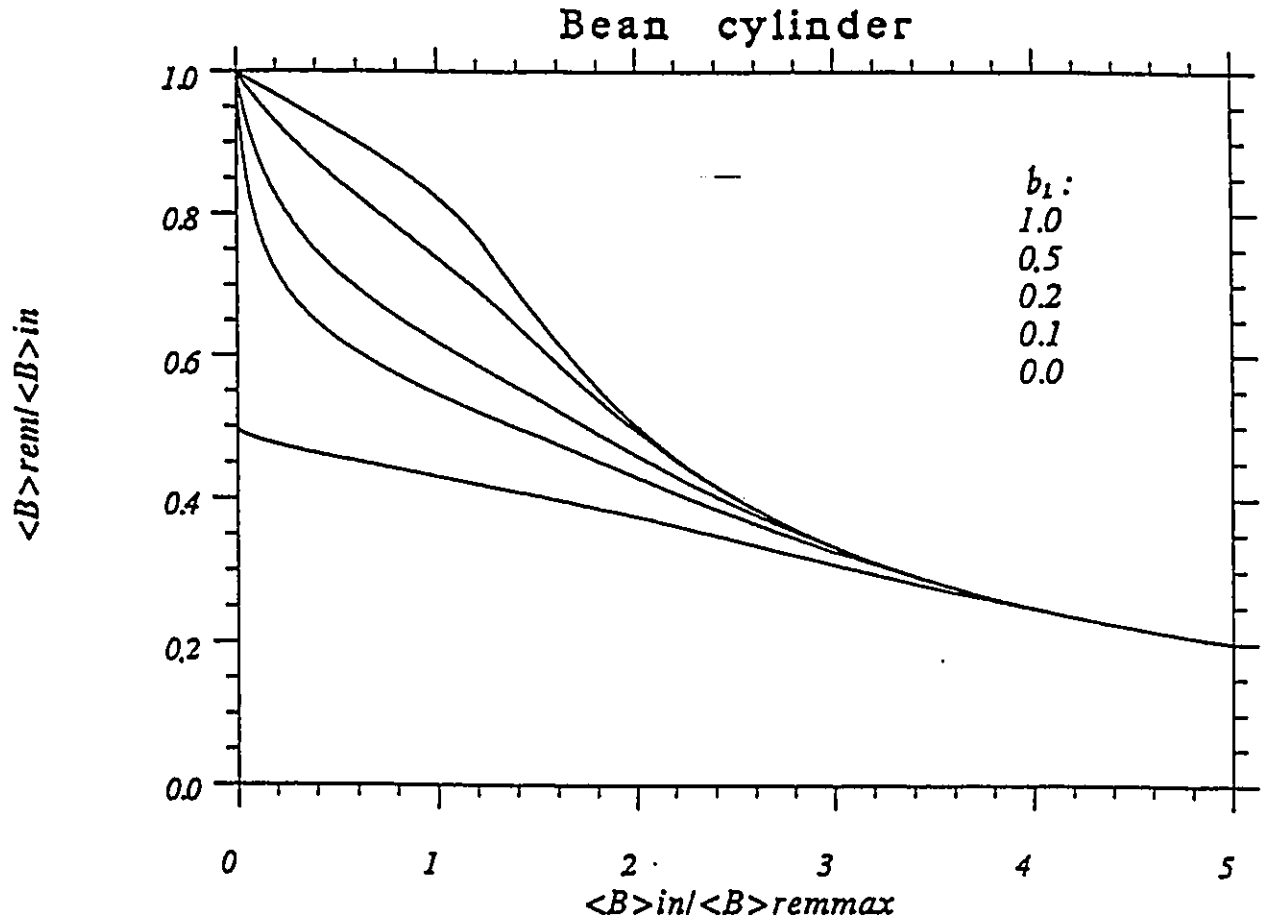

Figure 4.6: $< B >_{rem} / < B >_{in}$ vs $< B >_{in} / < B >_{remmax}$ for Bean cylinder with $b_1 = fB_{c1}/B_*$ varying from 1 to 0 from upper to lowermost curve

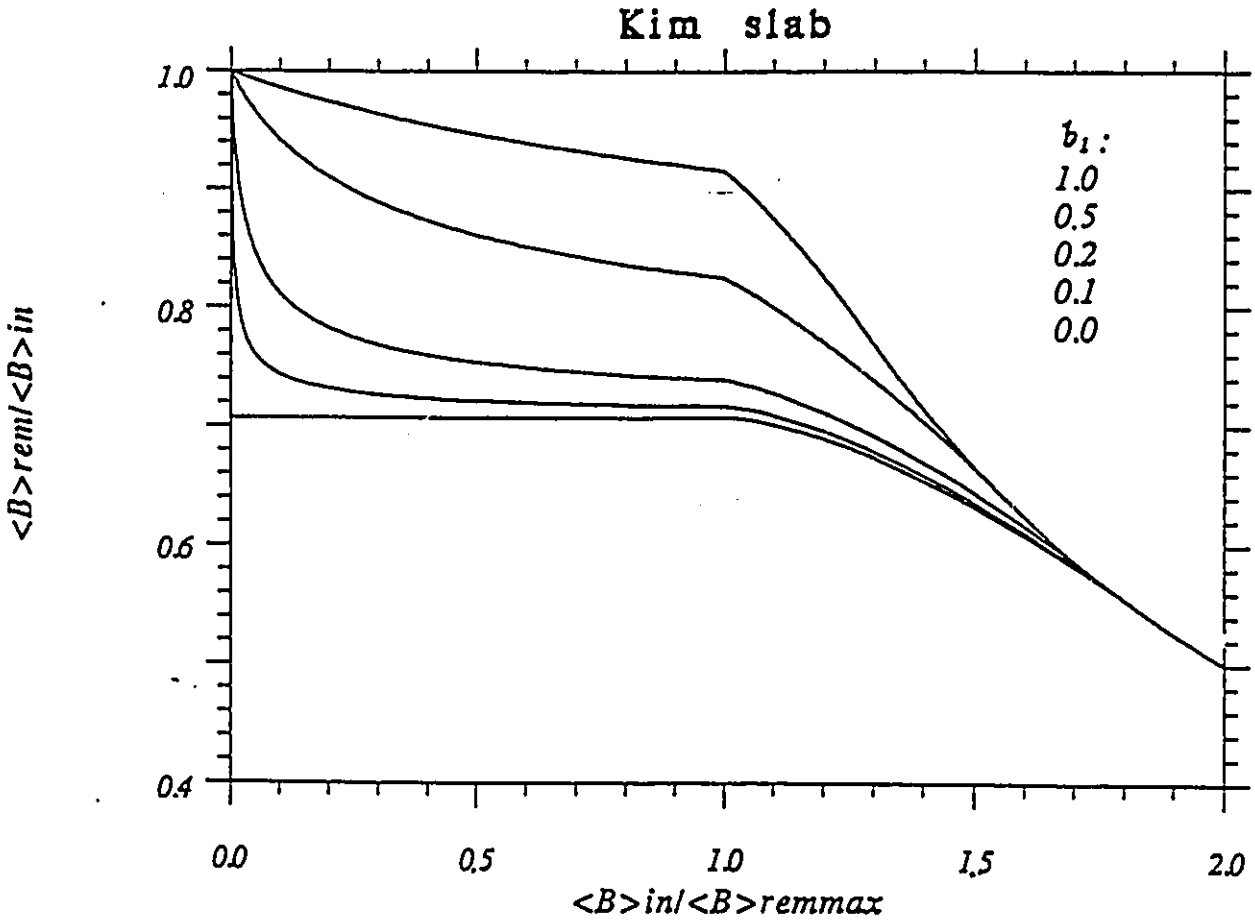

Figure 4.7: $< B >_{rem} / < B >_{in}$ vs $< B >_{in} / < B >_{remmax}$ for Kim slab with $b_1 = fB_{c1}/B_*$ varying from 1 to 0 from upper to lowermost curve

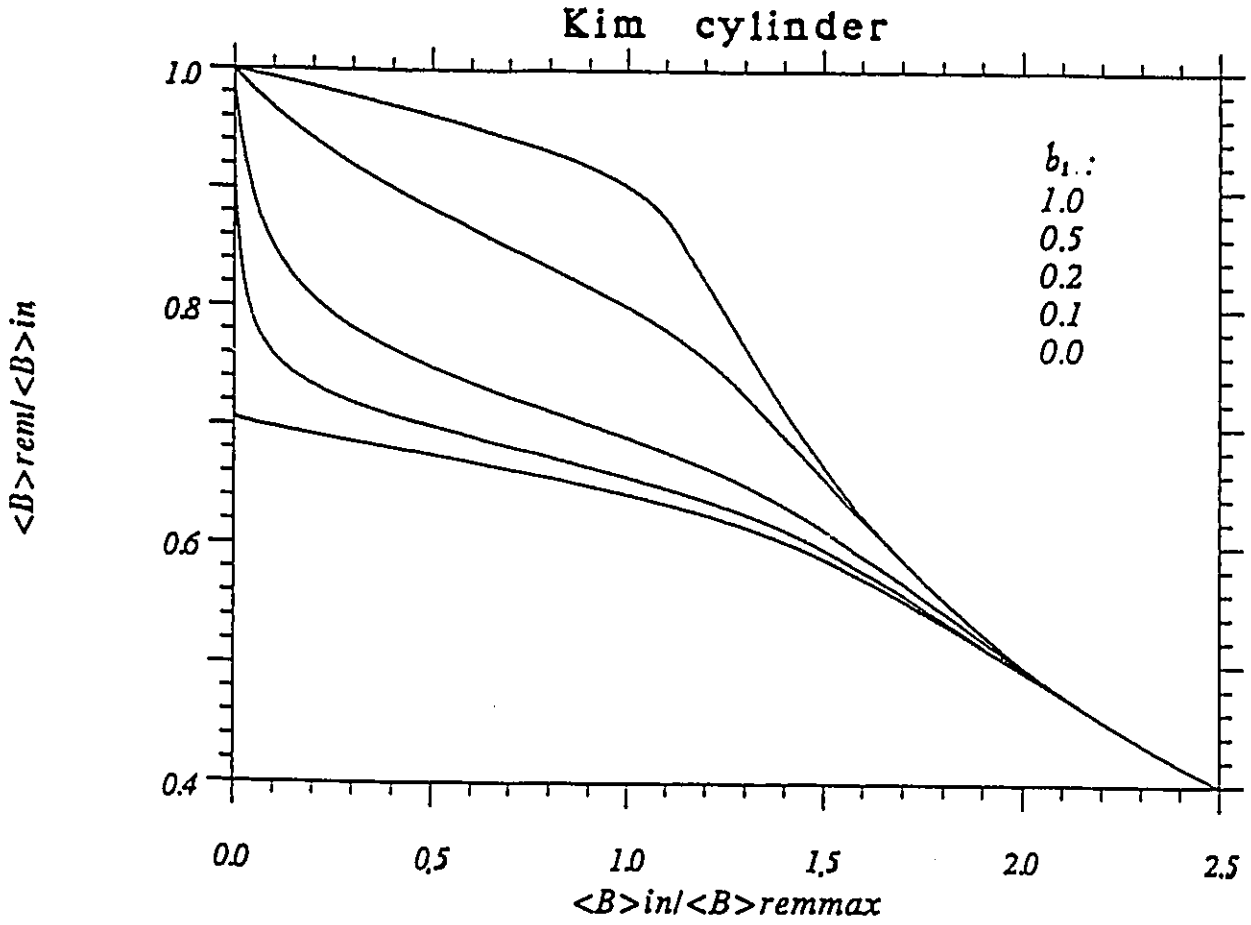

Figure 4.8: $< B >_{rem} / < B >_{in}$ vs $< B >_{in} / < B >_{remmax}$ for Kim cylinder with $b_1 = fB_{c1}/B_s$ varying from 0 to 1 from upper to lowermost curve

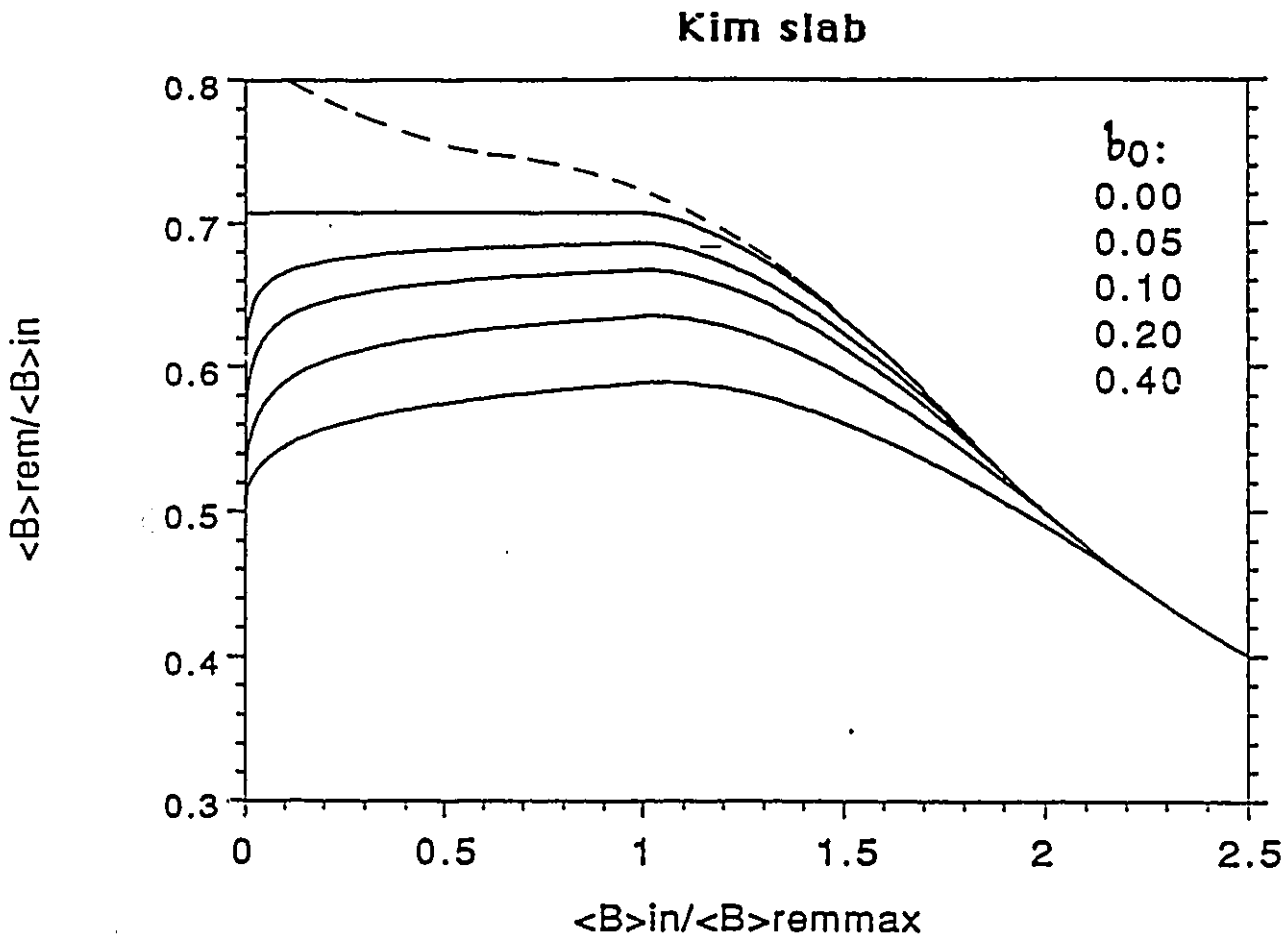

Figure 4.9: $< B >_{rem} / < B >_{in}$ vs $< B >_{in} / < B >_{remmax}$ for Kim slab with $b_1 = 0$ and $b_0 = B_0/B_*$ varying from 0 to 0.4 from upper to lowermost solid curves. The uppermost (dashed) curve shows the effect of a discontinuity b_1 ($= B_{c1}/B_* = 0.1$) when $b_0 = 0.4$ hence should be compared with the lowermost curve

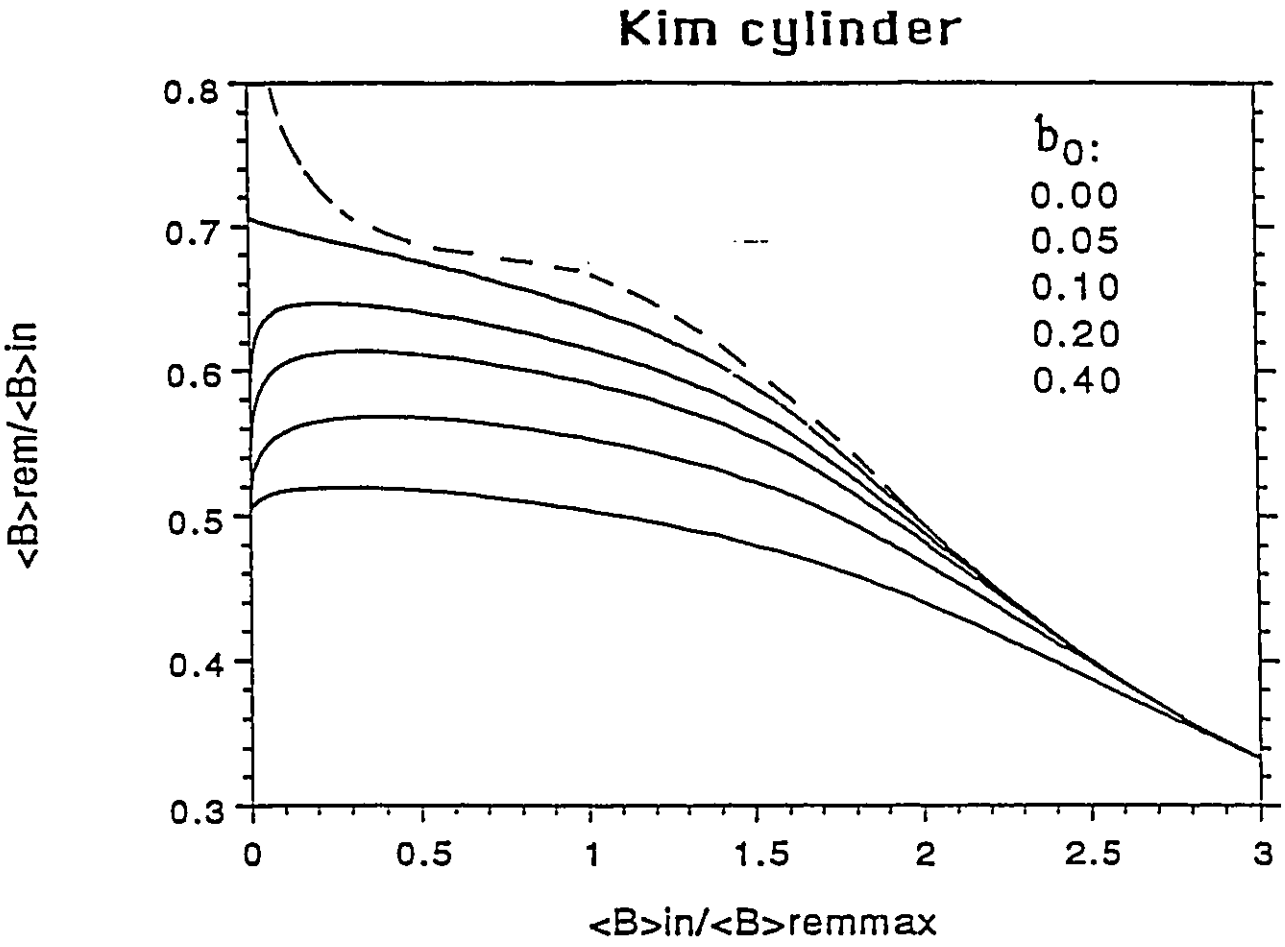

Figure 4.10: $< B >_{rem} / < B >_{in}$ vs $< B >_{in} / < B >_{remmax}$ for Kim cylinder with $b_1 = 0$ and $b_0 = B_0/B_*$ varying from 0 to 0.4 from upper to lowermost solid curve. The uppermost (dashed) curve shows the effect of a discontinuity b_1 ($= B_{c1}/B_* = 0.1$) when $b_0 = 0.4$ hence should be compared with the lowermost curve

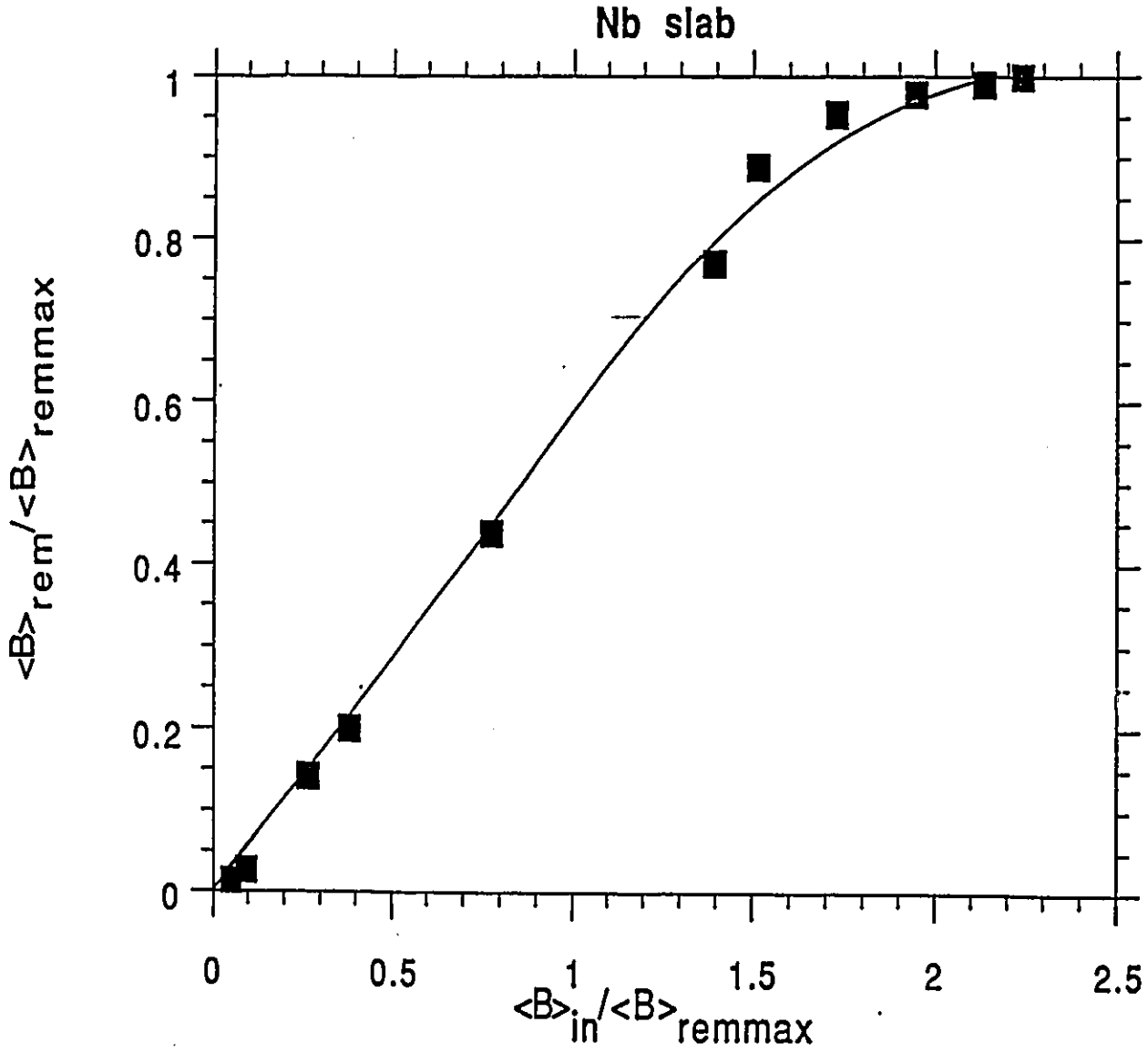

Figure 4.11: Nb slab in the format of $\frac{<B>_{rem}}{<B>_{remmax}}$ vs $\frac{<B>_{in}}{<B>_{remmax}}$ compared with Kim slab with $b_0 = B_0/B_* = 0.4$

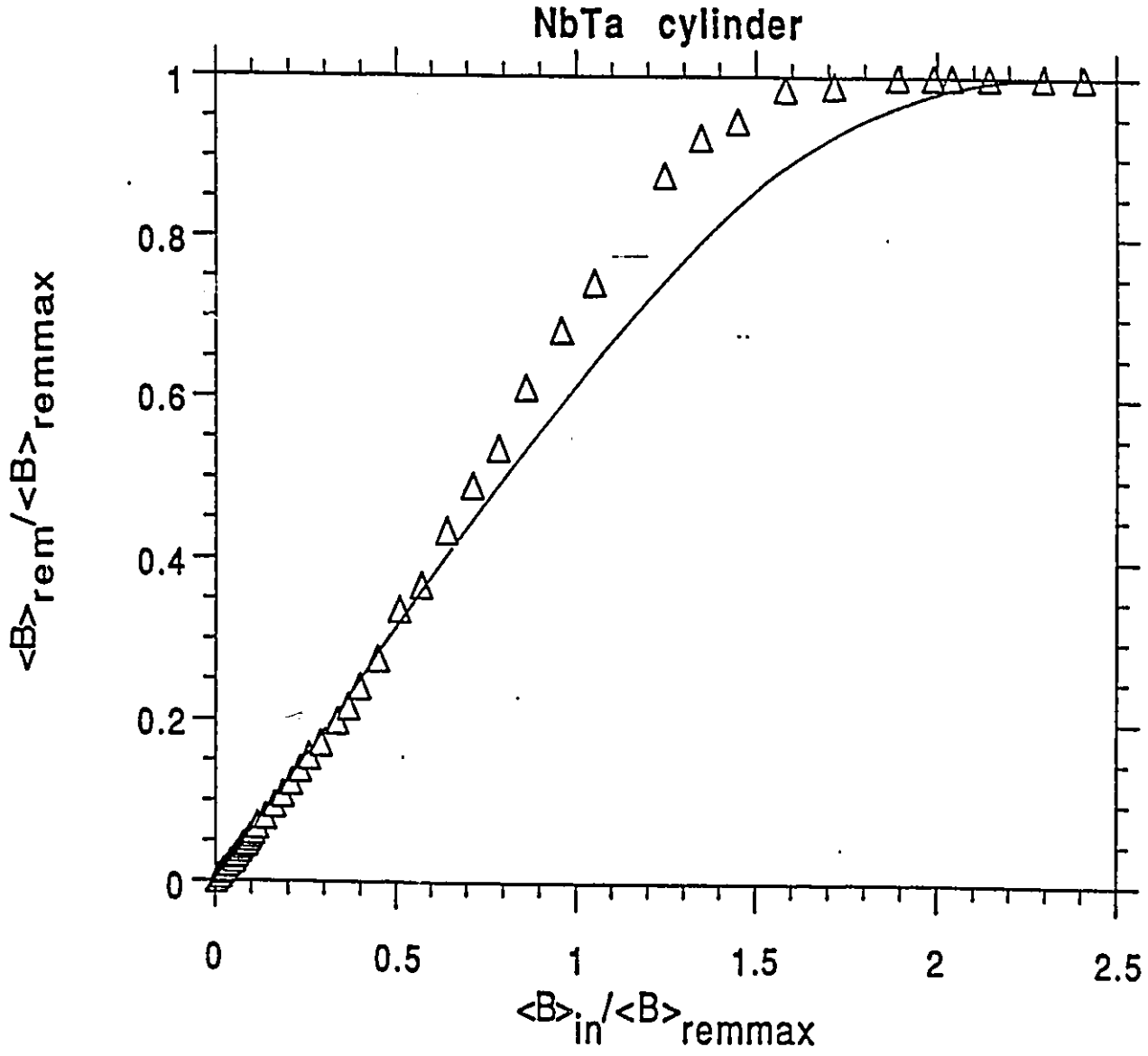

Figure 4.12: NbTa cylinder in the format of $\frac{<B>_{rem}}{<B>_{remmax}}$ vs $\frac{<B>_{in}}{<B>_{remmax}}$ compared with Kim cylinder with $b_0 = B_0/B_* = 0.15$

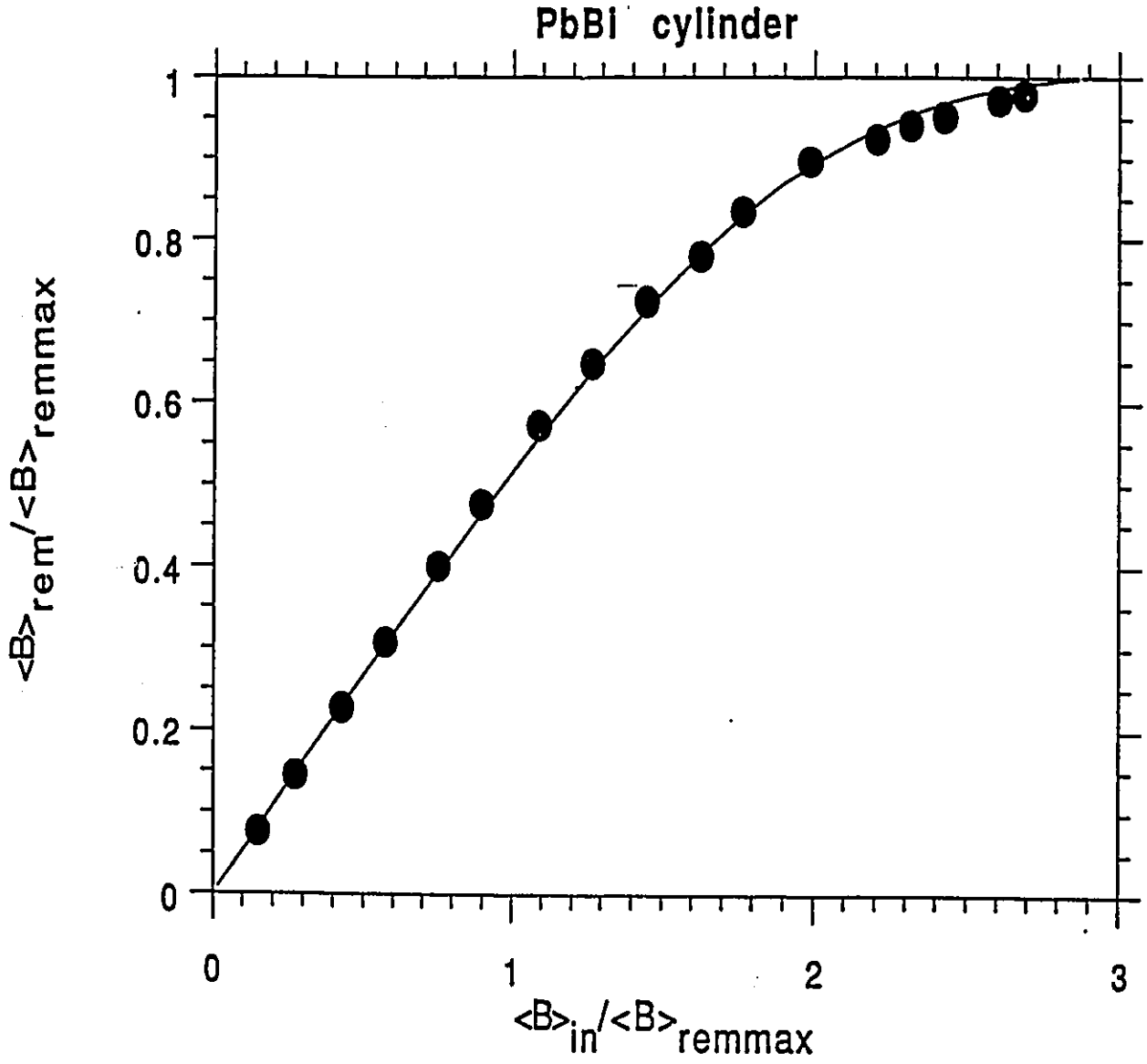

Figure 4.13: PbBi cylinder in the format of $\frac{<B>_{rem}}{<B>_{remmax}}$ vs $\frac{<B>_{in}}{<B>_{remmax}}$ compared with Kim cylinder with $b_0 = B_0/B_* = 0.35$

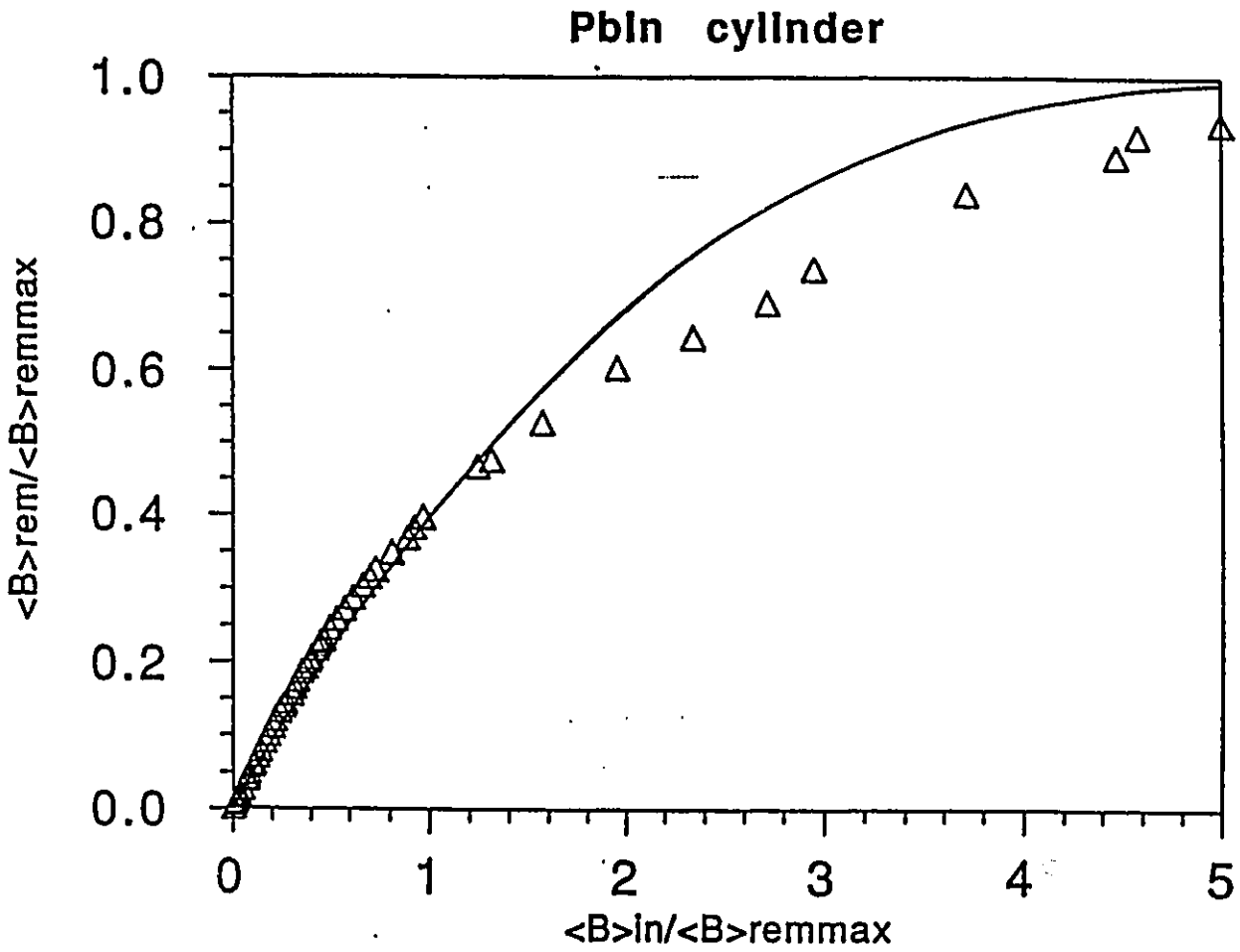

Figure 4.14: PbIn cylinder in the format of $\frac{<B>_{rem}}{<B>_{remmax}}$ vs $\frac{<B>_{in}}{<B>_{remmax}}$ compared with Bean cylinder

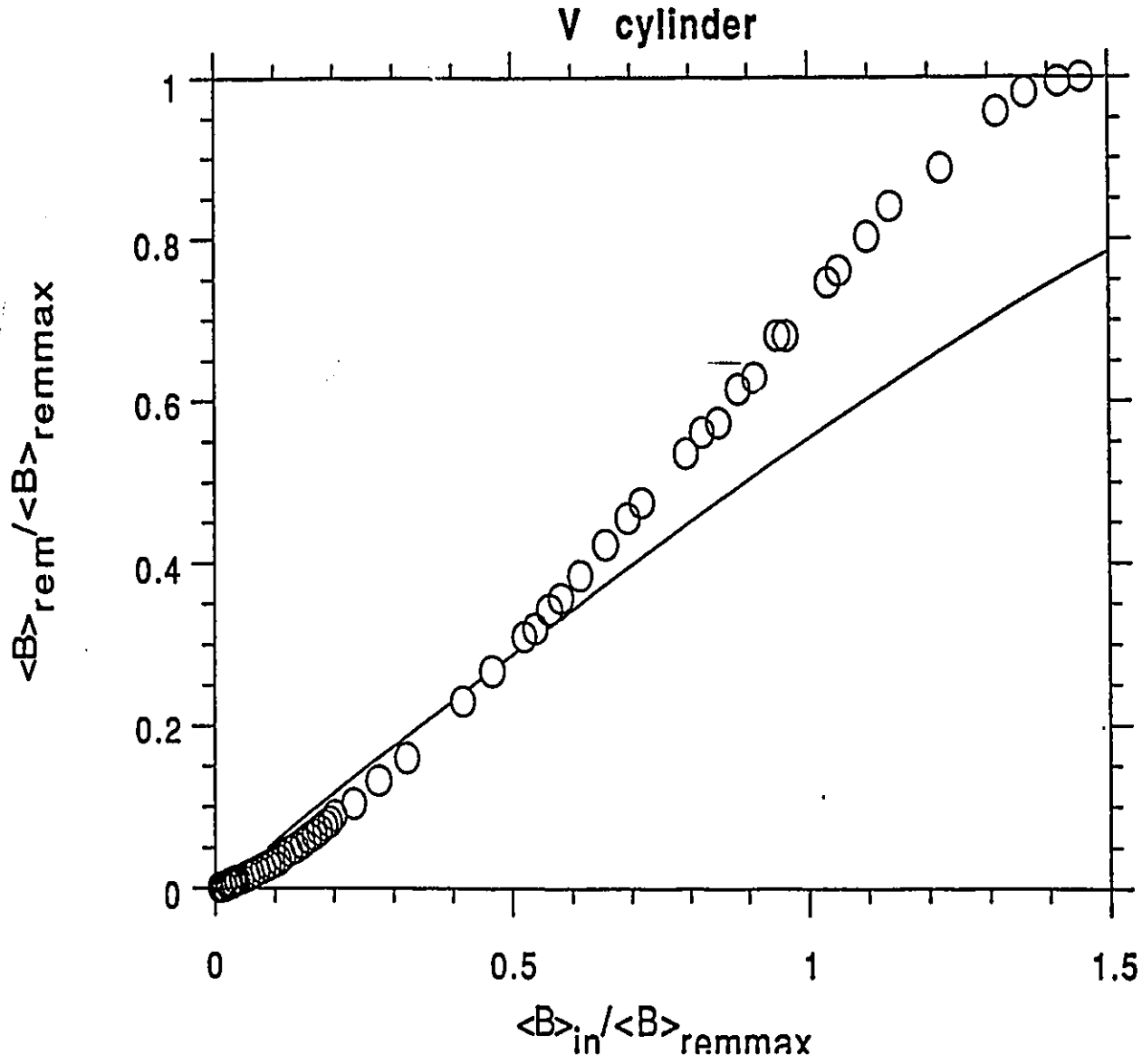

Figure 4.15: V cylinder in the format of $\frac{<B>_{rem}}{<B>_{remmax}}$ vs $\frac{<B>_{in}}{<B>_{remmax}}$ compared with Kim cylinder with $b_0 = B_0/B_* = 0.2$

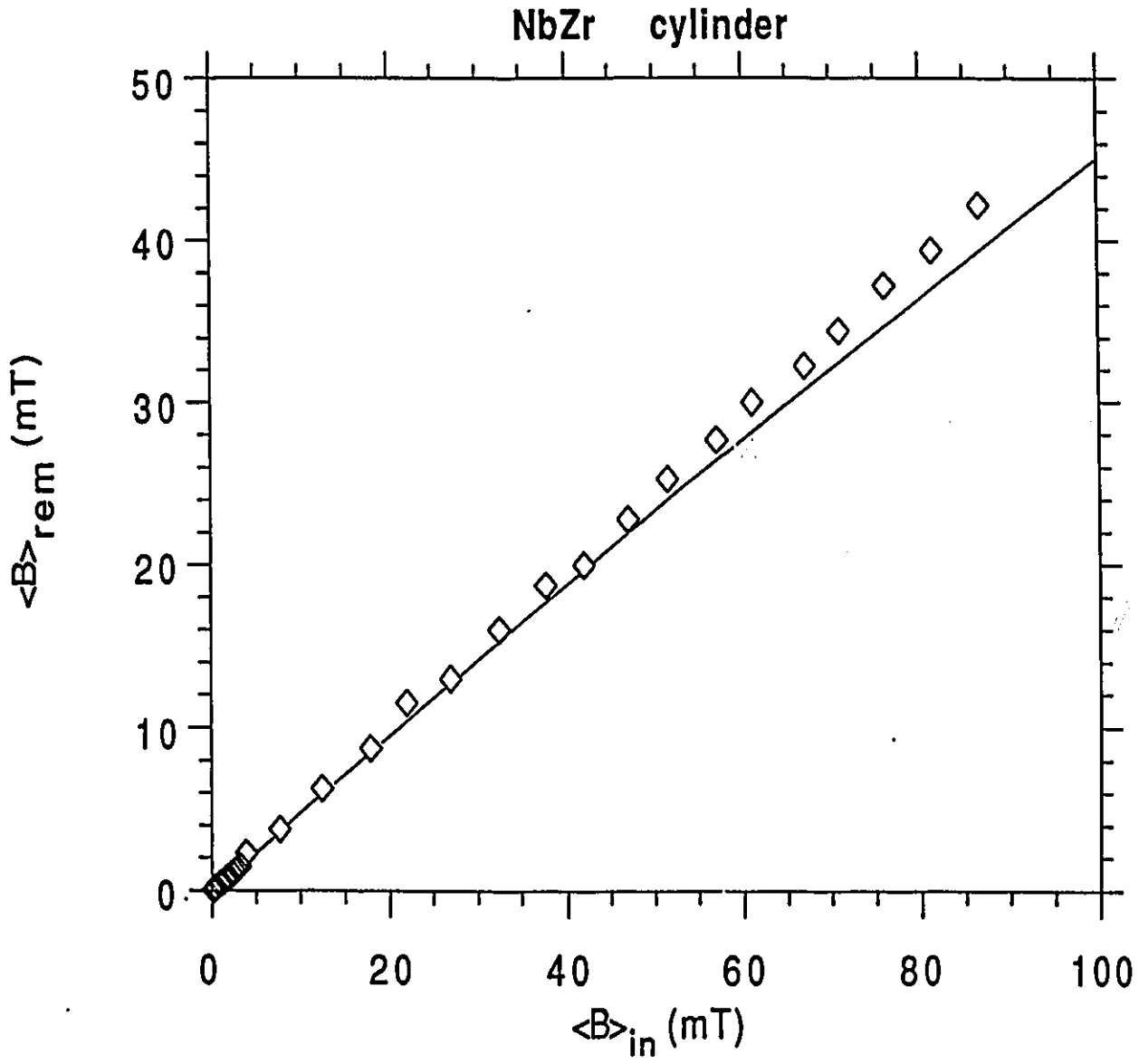

Figure 4.16: NbZr cylinder in the format of $< B >_{rem}$ vs $< B >_{in}$ compared with Bean cylinder

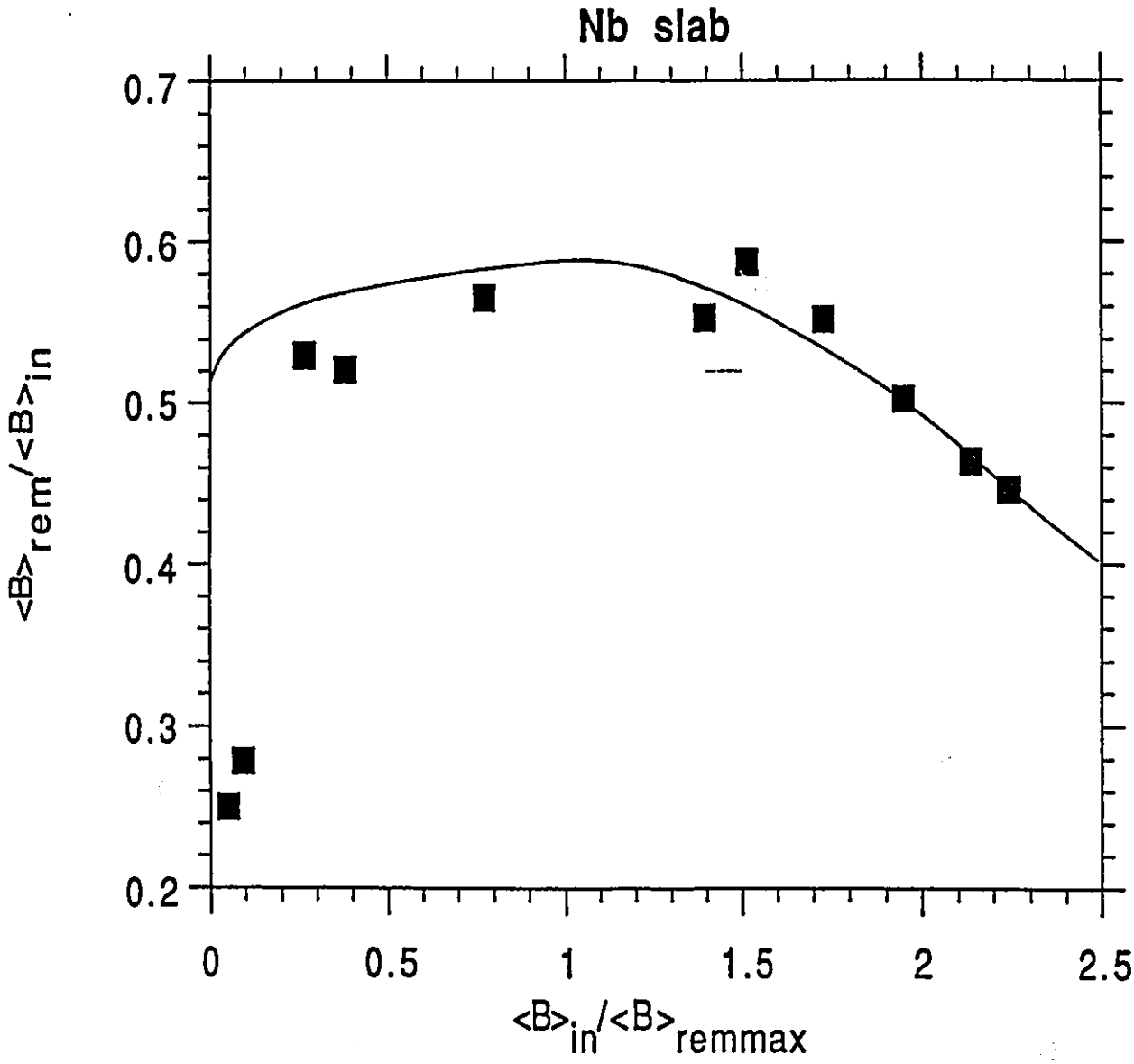

Figure 4.17: Nb slab in the format of $\frac{<B>_{rem}}{<B>_{in}}$ vs $\frac{<B>_{in}}{<B>_{remmax}}$ compared with Kim slab with $b_0 = B_0/B_* = 0.4$

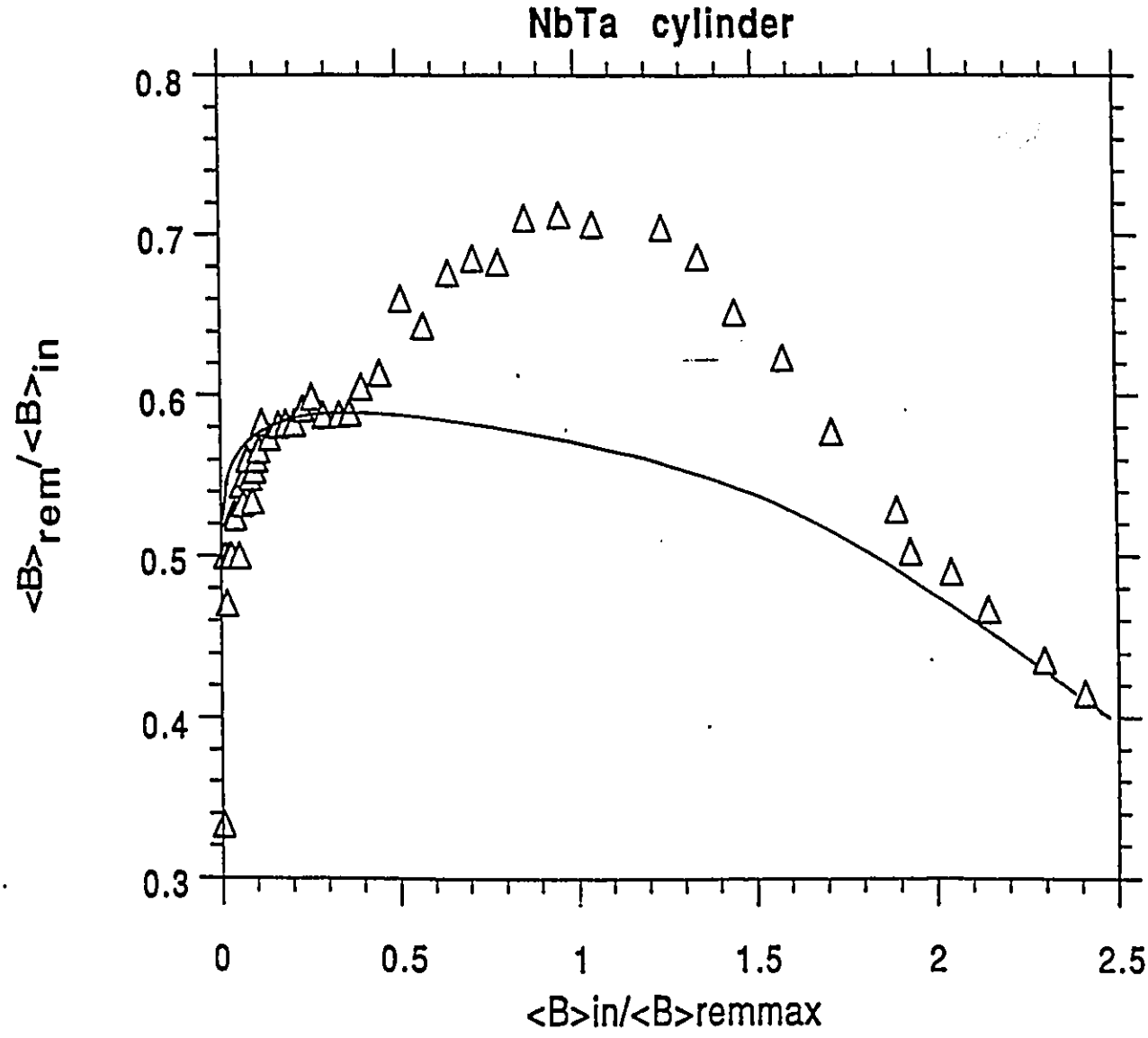

Figure 4.18: NbTa cylinder in the format of $\frac{<B>_{rem}}{<B>_{in}}$ vs $\frac{<B>_{in}}{<B>_{remmax}}$ compared with Kim cylinder with $b_0 = B_0/B_* = 0.15$

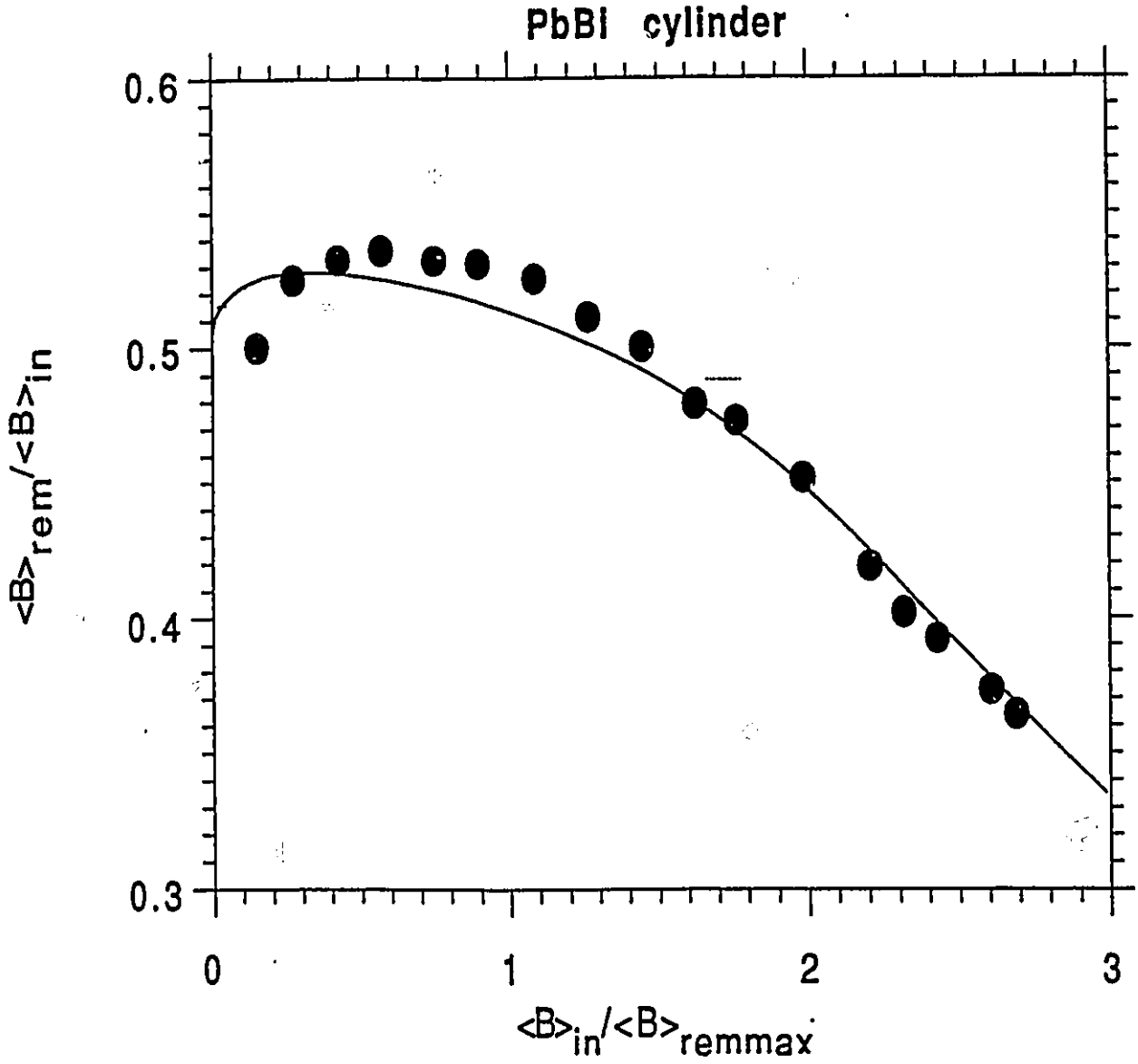

Figure 4.19: PbBi cylinder in the format of $\frac{<B>_{rem}}{<B>_{in}}$ vs $\frac{<B>_{in}}{<B>_{remmax}}$ compared with Kim cylinder with $b_0 = B_0/B_s = 0.35$

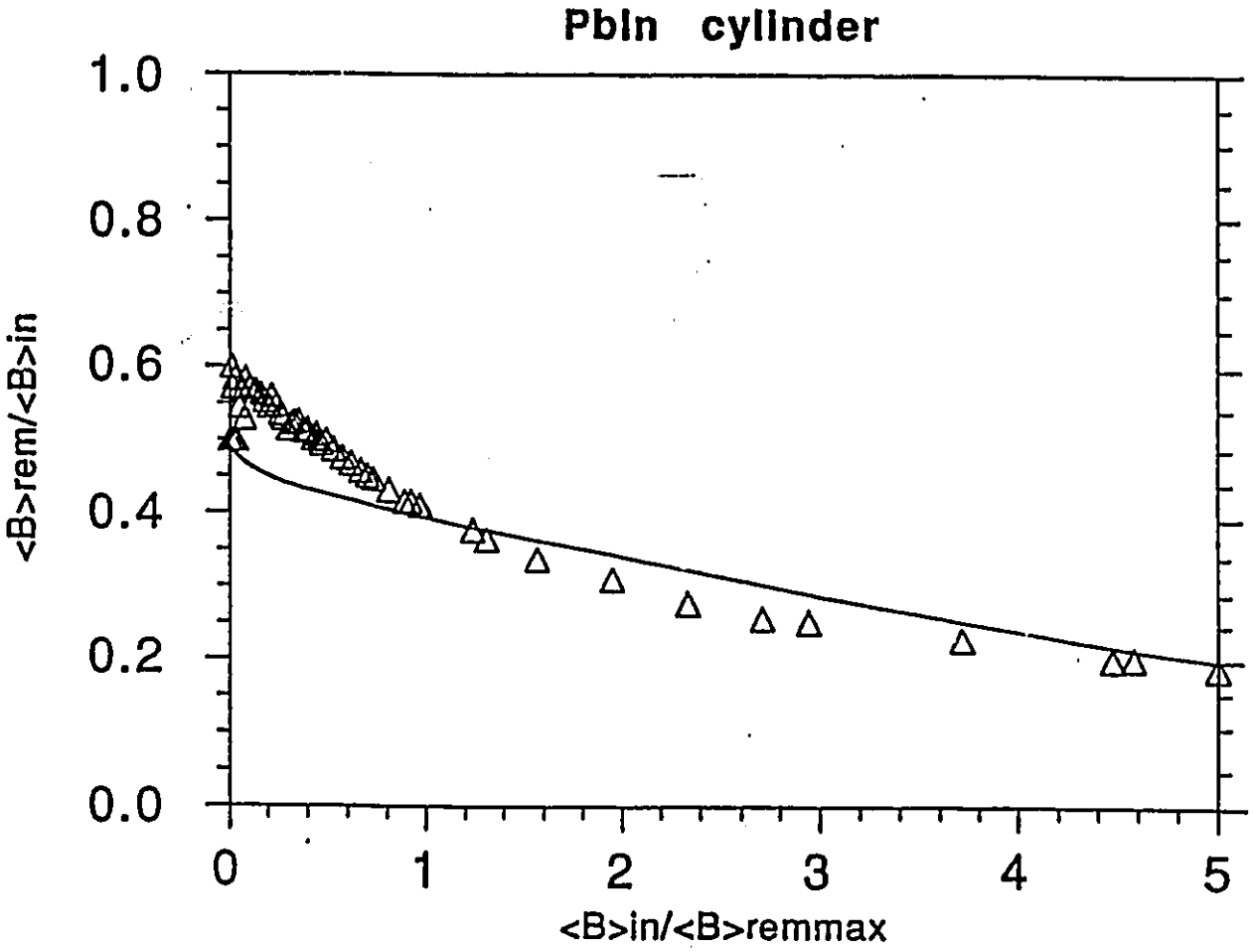

Figure 4.20: PbIn cylinder in the format of $\frac{<B>_{rem}}{<B>_{in}}$ vs $\frac{<B>_{in}}{<B>_{remmax}}$ compared with Bean cylinder

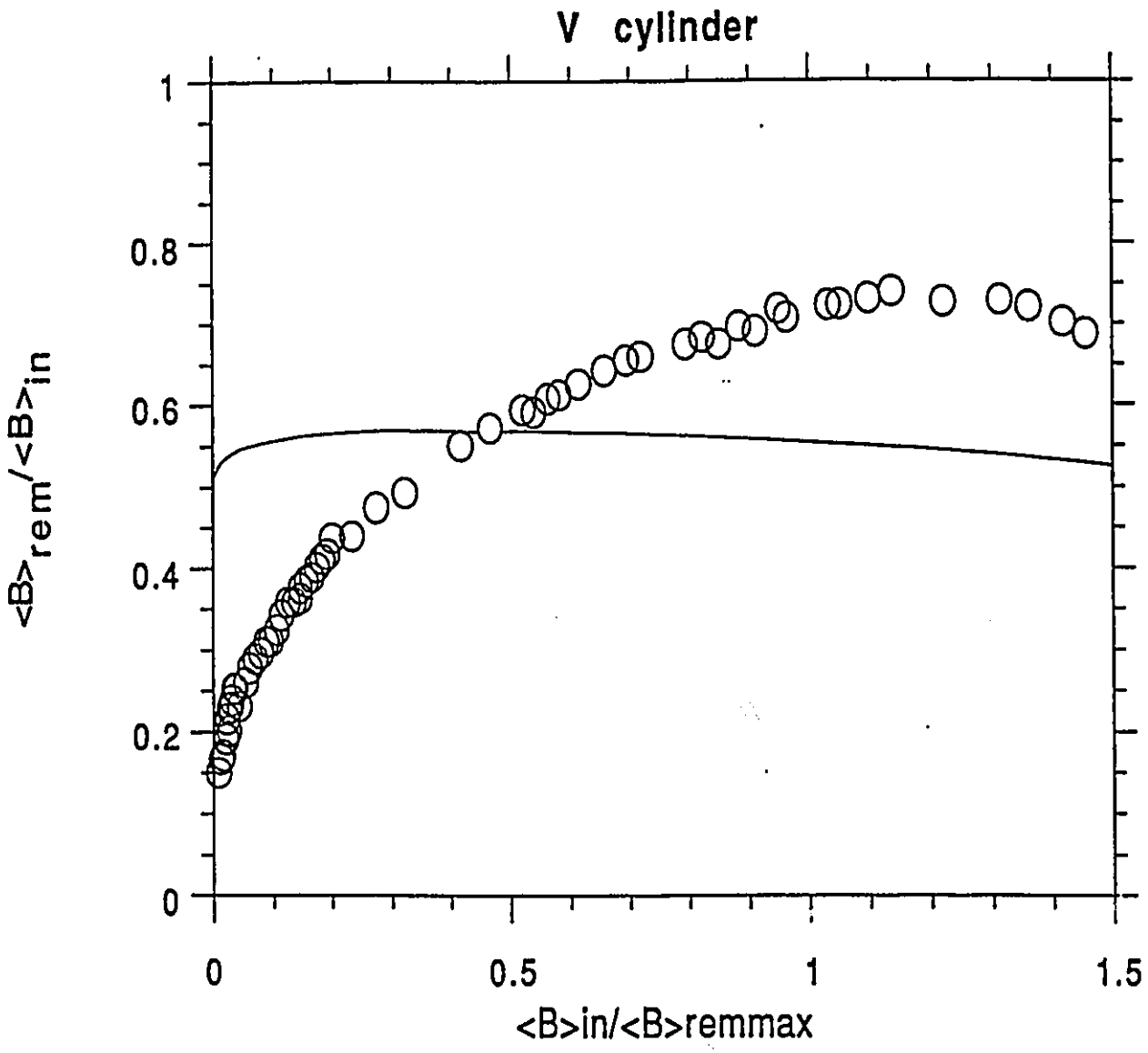

Figure 4.21: V cylinder in the format of $\frac{<B>_{rem}}{<B>_{in}}$ vs $\frac{<B>_{in}}{<B>_{remmax}}$ compared with Kim cylinder with $b_0 = B_0/B_* = 0.2$

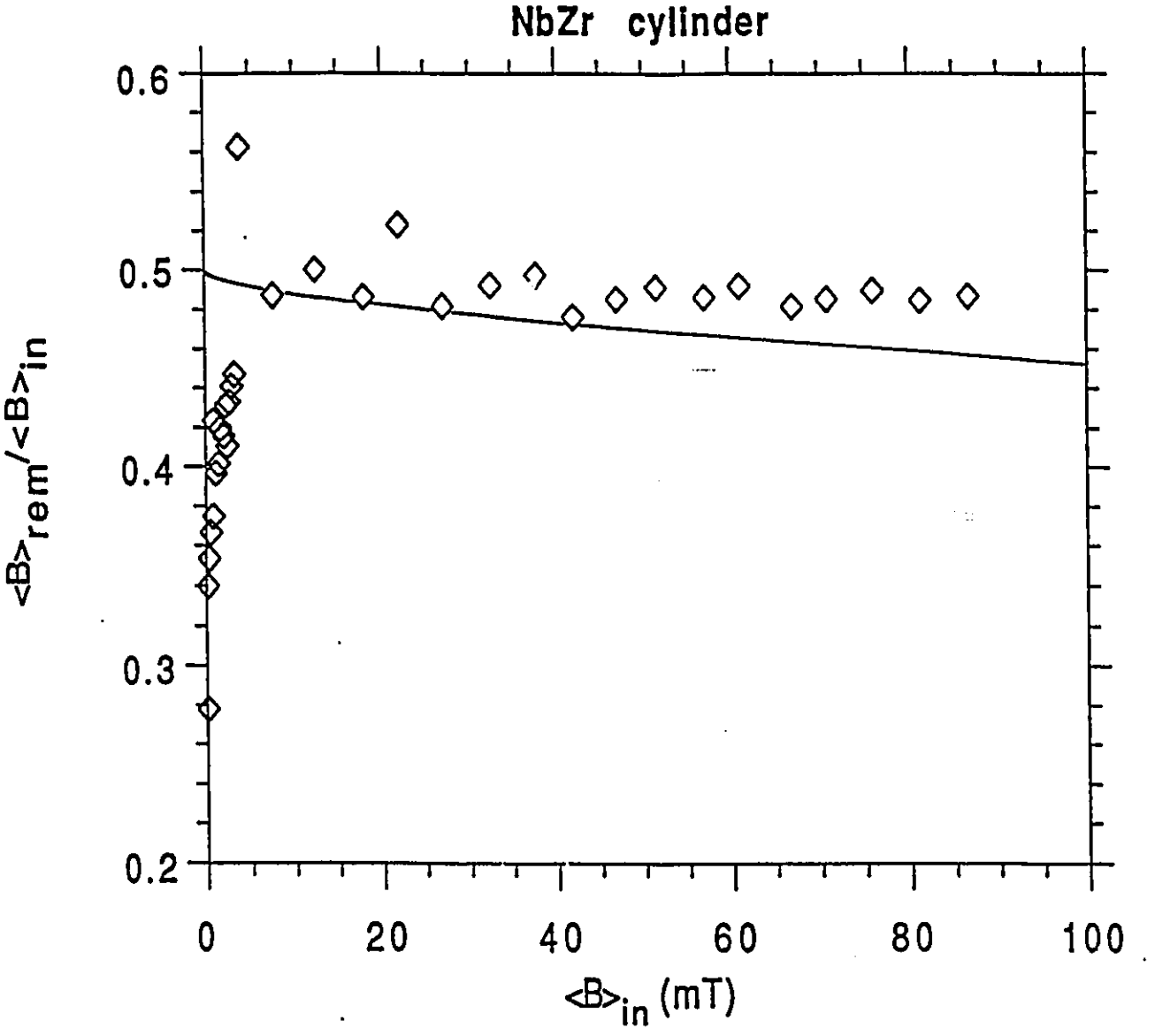

Figure 4.22: NbZr cylinder in the format of $< B >_{rem} / < B >_{in}$ vs $< B >_{in}$ compared with Bean cylinder with the assumption that $B_* = 500mT$

Appendix A

In this appendix we develop explicit expressions for $< B >_{in}$ and $< B >_{rem}$ for idealized planar and cylindrical geometry exploiting a prescription for the critical current density j_c of the frequently used form,

$$j_c = \frac{\alpha}{(B + B_0)^n} \tag{A.1}$$

valid when $B \ll B_{c2}$ where n>0, α and B_0 are temperature dependent parameters characterizing the specimen.

We consider,

(a) a slab infinite along the y and z axis of thickness $a = 2X$ with surfaces located at $x = \pm X$ and,

(b) an infinite long cylinder of radius R centered on the z axis.

The external magnetic field is directed along the z axis hence for a homogeneous,

isotropic specimen, the magnetic flux density reads,

$$\vec{B} = \hat{z}B_z(x) = \hat{z}B_z(r) \tag{A.2}$$

and the induced persistent current density

$$\vec{j} = \pm\hat{y}j_y(x) = \pm\hat{\Phi}j_\phi(r) \tag{A.3}$$

For convenience we will omit the subscripts y,z and Φ.

Maxwell's eqn $\nabla \times \vec{B} = \mu_0\vec{j_c}$ for our idealized geometry reads,

$$\frac{dB}{dx} = \mu_0 j(x), \qquad \frac{dB}{dr} = \mu_0 j(r) \tag{A.4}$$

Introducing the critical state assumption that wherever changes of magnetic flux density have occurred, the induced current exists in a critical state

$$j(x) = \pm j_c(B(x)), \qquad j(r) = \pm j_c(B(r)) \tag{A.5}$$

where j_c is given by eqn. A-1, leads to,

$$\frac{dB}{dx} = \pm\frac{\mu_0\alpha}{(B_0 + B)^n} = \frac{dB}{dr} \tag{A.6}$$

Integrating from x to X or from r to R in the volume where $j \neq 0$ (see Fig.A-1) eqn A-6 reads,

$$\int_x^X (B_0 + B)^n d(B_0 + B) = \pm\mu_0\alpha\int_x^X dx \tag{A.7.a}$$

$$\int_r^R (B_0 + B)^n d(B_0 + B) = \pm\mu_0\alpha\int_r^R dr \tag{A.7.b}$$

It is necessary now to identify boundary values and the zones where j flows in the + and − directions. Faraday's law of magnetic induction and previous history in the superconducting state determine the sign of j. We let $\mathfrak{B}_s$ denote the magnetic flux density just inside the specimen a distance of the order of λ from the surface. Thus the expressions for B(x) and B(r), (i.e. the B profiles) when H_a has been applied after zero field cooling and exceeds $H_{c1} + \Delta H_{cn}$ will not depend explicitly on H_a, nor on the magnitude of the Meissner surface current I_M and, nor on the magnitude of the surface barrier to flux entry ΔH_{cn}.

We let B_1 denote the 'discontinuities' in the B profiles. We assume that no 'extra' surface barrier exists to oppose the exit of magnetic flux after H_a has been applied and removed . However, if a dB/dH effect is postulated, hence a discontinuity in the B profile is assumed to exist, then $B_s = B_1$ under these circumstances (see right hand side of Fig. A-1).

To avoid repetition we focus on eqn. A-7(b) noting that substituting x for r and X for R in the formulae describes the B profiles for the infinite slab situated between the midplane and the surface at $x = X$. We let $B_1(r)$ denote the initial profile when $\mu_0 H_a$ is present and $B_2(r)$ the remanent profile in the volume where flux has been released when H_a was removed.

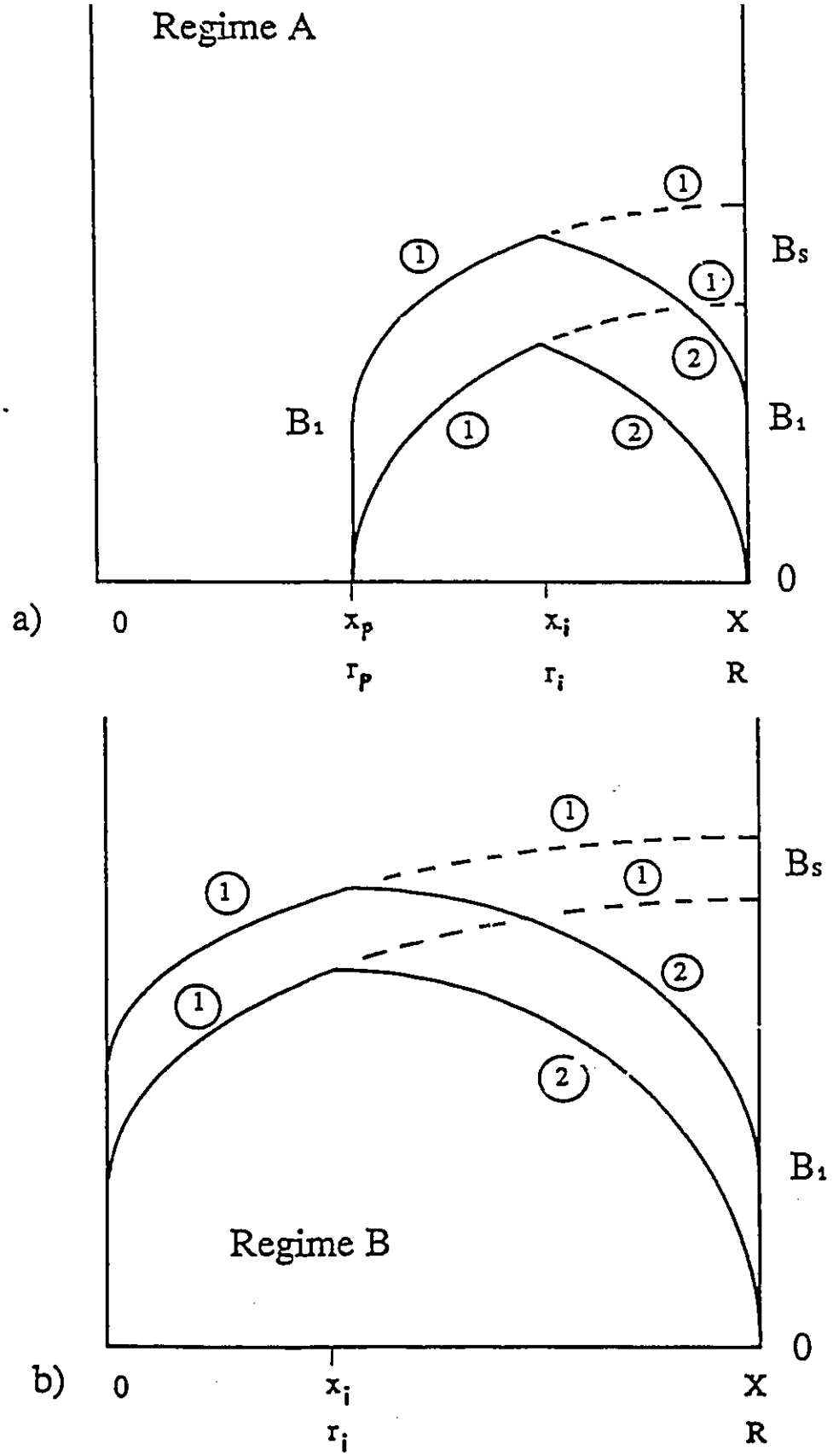

Figure A.1: Regimes A and B

Integrating eqn A-7(b) leads to,

$$(B_0 + B_s)^{n+1} - (B_0 + B_1(r))^{n+1} = B_*^{n+1}(1 - \frac{r}{R}) \tag{A.8}$$

for the $B_1(r)$ profiles (positive slope) and

$$(B_0 + B_1)^{n+1} - (B_0 + B_2(r))^{n+1} = -B_*^{n+1}(1 - \frac{r}{R}) \tag{A.9}$$

for the $B_2(r)$ profiles (negative slope).

Here for convenience we have written,

$$B_*^{n+1} = (n+1)\mu_0 \alpha R \tag{A.10}$$

We note that B_* corresponds to the first full penetration field when $B_0 = 0$ and $B_1 = 0$.

The position of the front of the advancing B profile is obtained from eqn A-8 since here,

$$B_1(r) = B_1(r_p) = B_1 \tag{A.11}$$

This leads to,

$$B_*^{n+1}(1 - \frac{r_p}{R}) = (B_0 + B_s)^{n+1} - (B_0 + B_1)^{n+1} \tag{A.12}$$

which is valid until r_p advances to the center and B_s attains the full penetration value B_s^* where,

$$B_s^* = [(B_0 + B_1)^{n+1} + B_*^{n+1}]^{1/(n+1)} - B_0 \tag{A.13}$$

which is obtained by letting $r_p = 0$ in eqn A-12. This is the first full penetration field when $B_0 \neq 0$ and $B_1 \neq 0$.

$B_1 = 0$ in eqns A-11,12 and 13 in the absence of a discontinuity in the B profiles. Eqn A-13 dictates the upper limit of regime A which applies over the range

$$0 < B_s \leq B_s^* \tag{A:14}$$

The position of the intersection of the $B_1(r)$ and $B_2(r)$ profiles is obtained by letting $r = r_i$ in eqns A-8 and A-9 and noting that,

$$B_1(r_i) = B_2(r_i) \tag{A.15}$$

Introducing eqns A-8 and A-9 into A-15 and solving for r_i leads to

$$B_s^{n+1}(1 - \frac{r_i}{R}) = \frac{(B_0 + B_s)^{n+1} - (B_0 + B_1)^{n+1}}{2} \tag{A.16}$$

Eqn A-16 is valid until r_i advances to the center and B_s attains a value B_s^{**} where,

$$B_s^{**} = [(B_0 + B_1)^{n+1} + 2B_s^{n+1}]^{1/(n+1)} - B_0 \tag{A.17}$$

which is obtained by letting $r_i = 0$ in eqn A-16. Eqn A-17 dictates the upper limit of regime B. We note that eqns A-8 and A-9 apply throughout regime A and B and when $B_s \gg B_s^{**}$.

Comparison of eqns A-12 and A-13 shows that,

$$1 - \frac{r_i}{R} = \frac{1}{2}(1 - \frac{r_p}{R}) \tag{A.18}$$

as expected from simple 'geometry' construction and consideration of Fig.A-1(a). Eqn A-18 is valid over the range $0 < B_a < B_s^*$. When full penetration of the advancing B profile has been achieved, hence r_p has reached the center, ($r_p = 0$), eqn A-18 no longer applies since now eqn A-12 is not valid over the entire range $0 < B_a \leq B_s^{**}$ (see Fig. A-1(b)).

$< B >_{in}$, the spatial average of the magnetic flux permeating the sample when $\mu_0 H_a$ is present, is obtained by introducing eqn A-12 in the form,

$$B_1(x) = B_1(r) = [(B_0 + B_s)^{n+1} - B_*^{n+1}(1 - \frac{r}{R})]^{1/(n+1)} - B_0 \qquad (A.19)$$

in the definitions,

$$< B >_{in} = \frac{1}{X} \int_{x_p}^{X} B_1(x) dx \qquad (A.20)$$

and

$$< B >_{in} = \frac{2}{R^2} \int_{r_p}^{R} B_1(r) r dr \qquad (A.21)$$

We note that $x_p = 0$, $r_p = 0$ for regime B.

$< B >_{rem}$, the spatial average of the magnetic flux threading the specimen after H_a has been removed is obtained by introducing eqn A-19 and A-9 in the form,

$$B_2(x) = B_2(r) = [(B_0 + B_1)^{n+1} + B_*^{n+1}(1 - \frac{r}{R})]^{1/(n+1)} - B_0 \qquad (A.22)$$

in the definitions,

$$< B >_{rem} = \frac{1}{X} \int_{x_p}^{x_i} B_1(x) dx + \frac{1}{X} \int_{x_i}^{X} B_2(x) dx \qquad (A.23)$$

and

$$< B >_{rem} = \frac{2}{R^2}\int_{r_p}^{r_i} B_1(r) r dr + \frac{2}{R^2}\int_{r_i}^{R} B_2(r) r dr \qquad (A.24)$$

Again we note that $x_p = 0$, $r_p = 0$ for regime B.

Bearing in mind that the limits of integration are determined by eqns A-12 and A-16 and that regime A corresponds to the range $0 < B_s \leq B_s^*$ (eqn A-13) and regime B to the range $B_s^* \leq B_s \leq B_s^{**}$ (eqn A-17), the definitions A-12,A-21,A-23 and A-24 together with the expressions for the B_1 and B_2 profiles (eqns A-19 and A-22) lead to the following formulae where, for brevity, we have introduced normalized quantities which we now define,

$$b_0 \equiv \frac{B_0}{B_*} \qquad b_1 \equiv \frac{fB_{c1}}{B_*} = \frac{B_1}{B_*} \qquad (A.25)$$

$$b_s \equiv \frac{B_s}{B_*} \qquad B_*^{n+1} = (n+1)\mu_0 \alpha R$$

Slab Geometry

Regime A

$$\frac{< B >_{in}}{B_*} = (b_0 + b_1)^{n+1}\left[\frac{b_0}{n+2} - \left(\frac{n+1}{n+2}\right)b_1\right] - (b_0 + b_s)^{n+1}\left[\frac{b_0}{n+2} - \left(\frac{n+1}{n+2}\right)b_s\right] \qquad (A.26)$$

Regime B

$$\frac{< B >_{in}}{B_*} = (\frac{n+1}{n+2})\{(b_0+b_s)^{n+2} - [(b_0+b_s)^{n+1}-1]^{(\frac{n+2}{n+1})}\} - b_0 \quad \text{(A.27)}$$

Regime A

$$\frac{< B >_{rem}}{B_*} = b_0[(b_0+b_1)^{n+1} - (b_0+b_s)^{n+1}] + \frac{2(n+1)}{n+2}\{[\frac{(b_0+b_s)^{n+1}}{2} + \frac{(b_0+b_1)^{n+1}}{2}]^{\frac{n+2}{n+1}} - (b_0+b_1)^{n+2}\} \quad \text{(A.28)}$$

Regime B

$$\frac{< B >_{rem}}{B_*} = (\frac{n+1}{n+2})\{2[\frac{(b_0+b_s)^{n+1}}{2} + \frac{(b_0+b_1)^{n+1}}{2}]^{\frac{n+2}{n+1}} - (b_0+b_s)^{n+2} - [(b_0+b_s)^{n+1}-1]^{\frac{n+2}{n+1}}\} - b_0 \quad \text{(A.29)}$$

Cylinder Geometry

It is now convenient to define the following quantities:

$$n_1 \equiv \frac{n+1}{2n+3} \qquad n_2 \equiv \frac{(n+1)^2}{(n+2)(2n+3)} \quad \text{(A.30)}$$

$$n_3 \equiv n_1 + n_2 \qquad n_4 = n_1 - n_2 \quad \text{(A.31)}$$

Regime A

$$\frac{< B >_{in}}{B_*} = b_0[(b_0+b_1)^{n+1}-(b_0+b_s)^{n+1}][2+(b_0+b_1)^{n+1}-(b_0+b_s)^{n+1}] + 2[n_3-n_2(b_0+b_s)^{n+1}](b_0+b_s)^{n+2}-2[n_3+n_1(b_0+b_1)^{n+1} - n_3(b_0+b_s)^{n+1}](b_0+b_1)^{n+2} \quad (A.32)$$

Regime B

$$\frac{< B >_{in}}{B_*} = 2[n_3-n_2(b_0+b_s)^{n+1}](b_0+b_s)^{n+2}+2n_2[(b_0+b_s)^{n+1}-1]^{\frac{1}{n_1}}-b_0 \quad (A.33)$$

Regime A

$$\frac{< B >_{rem}}{B_*} = [2+(b_0+b_1)^{n+1}-(b_0+b_s)^{n+1}]\{(b_0+b_1)^{n+1}[b_0-2n_3(b_0+b_1)] - b_0(b_0+b_s)^{n+1}\}+2[\frac{(b_0+b_1)^{n+1}}{2}+\frac{(b_0+b_s)^{n+1}}{2}]^{\frac{n_1}{n_2}} \{2n_3+(1+n_2)[(b_0+b_1)^{n+1}-(b_0+b_s)^{n+1}]\} \quad (A.34)$$

Regime B

$$\frac{< B >_{rem}}{B_*} = b_0[1+(b_0+b_1)^{n+1}-(b_0+b_s)^{n+1}][(b_0+b_1)^{n+1}-(b_0+b_s)^{n+1}]$$

$$+2[\frac{(b_0+b_1)^{n+1}}{2}+\frac{(b_0+b_s)^{n+1}}{2}]^{\frac{n_1}{n_2}}$$

$$\{2n_3+n_1[(b_0+b_1)^{n+1}-(b_0+b_s)^{n+1}]\}+2n_2$$

$$[(b_0+b_s)^{n+1}-1]^{\frac{1}{n_1}}-2[n_3+n_2(b_0+b_1)^{n+1}](b_0+b_1)^{n+2}$$

$$-b_0[1+\frac{(b_0+b_1)^{n+1}}{2}-\frac{(b_0+b_s)^{n+1}}{2}]^2 \qquad \text{(A.35)}$$

Table I is readily calculated letting $n = 0$ (Bean) and $n = 1$ (Kim approximation) and $B_0 = 0$ is the above formulae and evaluating these at the limit where $B_s = B_s^{**}$ (eqn A-17).

Bibliography

[1] A.A.Abrikosov, *Zh.Eksp.Teor.Fiz.*32,1442(1957).Translation:*Sov.Phys.-JETP* 5,1174(1957)

[2] P.W.Anderson, *Phys.Rev.Lett.* 9,309(1962)

[3] P.W.Anderson and Y.B.Kim, *Rev.Mod.Phys.* 36,39(1964)

[4] C.P. Bean, *Rev.Mod.Phys.* 36,31(1964)

[5] L.Burlachkov, Y.Yeshurun, M.Konczykowski and F.Holtzberg, *Phys.Rev.* B45,8193-(1992)

[6] A.M.Campbell and J.E. Evetts, *Adv.Phys.* 21,199(1972)

[7] J.E. Evetts and A.M.Campbell *Proc.10th Intern. Conf. Low Temp. Phys.* Vol II B(Moscow,Veniti)p.33(1966)

[8] J.R.Clem, *J.Appl. Phys.* 50(1),3518(1979)

[9] J.Friedel, P.G.de Gennes and J.Matricon, *Appl.Phys.Lett.* 2,199(1963)

[10] G.Gandolfini, *M.Sc.Thesis*,U. of Ottawa (1989)

[11] S.H.Goedemoed, A.van der Giessen, D.DeKlerk and C.J.Gorter, *Phys.Letters* 3, 250-(1963)

[12] J.A.Hulbert, *Brit.J.Appl.Phys.* 16,1657(1965)

[13] R.Job and M.Rosenberg, *Physica C* 172,391(1991)

[14] Y.B.Kim, C.F.Hempstead and A.R.Strnad, *Phys.Rev.Lett.*9,306(1962); *Phys.Rev.* 129,528(1963)

[15] L.Krusin-Elbaum, A.P.Malozemoff, Y.Yeshurun, D.C.Cronemeyer and F.Holtzberg, *Phys.Rev.* B39,2936(1989)

[16] L.Krusin-Elbaum, A.P.Malozemoff, D.C.Cronemeyer, F.Holtzberg, J.R.Clem - Z.D.Hao *J.Appl.Phys.* 67,4670(1990)

[17] M.A.R.LeBlanc and D.J.Griffiths, *Appl.Phys.Letters* 9,131(1966)

[18] M.A.R.LeBlanc, G.Fillon, W.E.Timms, A.Zahradnitsky and J.R.Cave, *Cryogenics* 21,491(1981)

[19] H.London, *Phys.Letters* 6,162(1963)

[20] M.W.McElfresh, Y.Yeshurun, A.P.Malozemoff and F.Holtzberg, *Physica A* 169,308-(1990)

[21] M.A-K.Mohamed, J.Jung and J.P.Franck, *Phys.Rev.* B39,9614(1989)

[22] M.A-K.Mohamed, J.Jung and J.P.Franck, *Phys.Rev.* B41,4286(1990)

[23] M.A-K.Mohamed, J.Jung and J.P.Franck, *Phys.Rev.* B41,6466(1990)

[24] M.A-K.Mohamed, J.Jung and J.P.Franck, *Phys.Rev.* B42,6181(1990)

[25] V.V.Moshchalkov, J.Y.Henry, C.Marin, J.Rossat-Mignod and J.F.Jacquot, *Physica C* 175,407(1991)

[26] G.Ravi Kumar and P.Chaddah, *Phys.Rev.* B39,4704(1989)

[27] Th.Ritzi, Ch.Heinzel, Ch.Neumann and P.Ziemann, *Appl.Phys.Lett.* 60,2297(1992)

[28] P.Svedlindh, K.Niskanen, P.Norling, P.Nordblad, L.Lundgren, C.Rossel, M.Sergent, R.Chevrel and M.Potel, *Phys.Rev.* B43,2735(1991)

[29] H.Ullmaier, *Irreversible Properties of Type II Superconductors* , Springer-Verlag, Berlin(1975)

[30] K.Yasukochi, T.Ogasahara, N.Usui and S.Ushio, *J.Phys.Soc.Jpn.* 19,137(1964)

[31] K.Yasukochi, T.Ogasahara, N.Usui, H.Kobayashi and S.Ushio, *J.Phys.Soc.Jpn.* 21,-89(1966)

[32] Y.Yeshurun, A.P.Malozemoff, F.Holtzberg and T.R.Dinger, *Phys.Rev.* B 38,11828-(1988)

[33] M.Xu, *Phys.Rev.* B 44,2713(1991)

[34] M.Xu, D.Shi and R.Fox, *Phys.Rev.* B 42,10773(1990)